



**HAL**  
open science

## Hygrothermal performance of multilayer wall assemblies incorporating starch/beet pulp in France

Elias Harb, Chadi Maalouf, Christophe Bliard, Elias Kinab, Mohammed Lachi, Guillaume Polidori

### ► To cite this version:

Elias Harb, Chadi Maalouf, Christophe Bliard, Elias Kinab, Mohammed Lachi, et al.. Hygrothermal performance of multilayer wall assemblies incorporating starch/beet pulp in France. *Construction and Building Materials*, 2024, 445, pp.137773. 10.1016/j.conbuildmat.2024.137773 . hal-04683385

**HAL Id: hal-04683385**

**<https://hal.science/hal-04683385v1>**

Submitted on 26 Sep 2024

**HAL** is a multi-disciplinary open access archive for the deposit and dissemination of scientific research documents, whether they are published or not. The documents may come from teaching and research institutions in France or abroad, or from public or private research centers.

L'archive ouverte pluridisciplinaire **HAL**, est destinée au dépôt et à la diffusion de documents scientifiques de niveau recherche, publiés ou non, émanant des établissements d'enseignement et de recherche français ou étrangers, des laboratoires publics ou privés.



Distributed under a Creative Commons Attribution - NonCommercial - NoDerivatives 4.0 International License



# Hygrothermal performance of multilayer wall assemblies incorporating starch/beet pulp in France

Elias Harb<sup>a,\*</sup>, Chadi Maalouf<sup>a</sup>, Christophe Bliard<sup>b</sup>, Elias Kinab<sup>c</sup>, Mohammed Lachi<sup>a</sup>, Guillaume Polidori<sup>a</sup>

<sup>a</sup> Laboratoire de MATériaux et Ingénierie Mécanique, MATIM, Université de Reims-Champagne-Ardenne URCA, Moulin de la Housse, Reims Cedex 2 51687, France

<sup>b</sup> Institut de Chimie Moléculaire de Reims, ICMR-UMR 7312 CNRS, Université de Reims-Champagne-Ardenne URCA, Moulin de la Housse, Reims Cedex 2 51687, France

<sup>c</sup> Université Libanaise, Faculté de Génie, Branche II, Roumieh, Lebanon

## ARTICLE INFO

### Keywords:

Beet pulp  
Starch  
Bio-insulation material  
Hygrothermal properties  
Numerical simulation  
WUFI®Bio  
WUFI® Plus

## ABSTRACT

This work focuses on the investigation of the hygrothermal performance of four different wall insulation assemblies including starch/beet pulp composite for an office in France under two climatic conditions. Subsequently, a comparative performance analysis is made on all studied assemblies by substituting the Starch/beet pulp composite with hemp concrete (HC). For each design, the overall energy performance, total water content, drying rate and condensation risk were evaluated through hygrothermal simulations using the WUFI® Plus software and mold growth risk assessment was conducted with WUFI®Bio software. Results showed that insulation assemblies based on Starch/Beet pulp exhibited a slightly improved effectiveness in potential energy savings and higher dryness rate while having a higher condensation risk, a lower dynamic thermal performance, and a higher susceptibility to mold growth risk. Moreover, insulation assemblies based on Starch/Beet pulp demonstrated better hygrothermal performance under Nancy's climate compared to that of Marseille. Wall assemblies based on hemp concrete reduced total energy consumption by up to 35 % in Nancy's climate and 24.9 % in Marseille's climate. In comparison, starch/beet pulp concrete achieved reductions of up to 37.5 % and 26 % respectively. However, the mold growth risk for starch/beet pulp was 1.2–7.2 times higher than for hemp concrete. In Marseille's climate, this risk was 2.3–8.9 times higher for starch/beet pulp and 4.7–17.8 times higher for hemp concrete compared to Nancy's climate. The findings from these room-scale studies enhance the understanding of the hygrothermal behavior of the Starch/Beet pulp bio-composite material by comparing its performance, under the same conditions, to that of the well-studied hemp concrete material in the literature. Additionally, these studies provide greater insight into the impact of water on the overall energy consumption, service performance of a building and health hazards. Finally, this research also tackles the challenges of integrating innovative materials into the established construction industry.

## 1. Introduction

The building sector is undoubtedly a massive energy consumer and a main contributor to greenhouse gas emissions across the globe. For instance, at the EU level, buildings account for 40 % of the total energy consumption and 36 % of greenhouse gas emissions [1]. While 60 % of the total consumed energy in buildings is used for space heating and cooling [2], over 50 % of energy demand is due to the heat losses through the building envelope and therefore is deemed as a critical element for enhancing buildings thermal performance [3].

Successive thermal regulations (RT 1974, RT1982, RT1988, RT2000,

RT2005, RT2012) were introduced in France targeting at first continuous reduction in building energy consumption from 300 kWh/m<sup>2</sup>/year to less than 50 kWh/m<sup>2</sup>/year and lately promoting green constructions [4]. Recently, a new environmental regulation RE2020 in force from January 2022, introduced new environmental standards. It has three main objectives: improving energy performance and further reducing energy consumption in new buildings, reducing carbon footprint and global emissions of new buildings, and finally guaranteeing comfort in hot weather as heat waves are expected to become increasingly frequent [5].

Although the thermal properties of insulation materials and building envelope are crucial for energy saving, hygroscopic properties must be

\* Corresponding author.

E-mail address: [elias.m.harb@gmail.com](mailto:elias.m.harb@gmail.com) (E. Harb).

Symbols			
S/BP	Starch/Beet Pulp	$\delta$	Water vapour permeability of specimen (kg/(m s Pa))
HC	Hemp concrete	$\Delta p_v$	Water vapour pressure difference across specimen (Pa)
D	Diameter (m)	$P_{sat}$	Water vapour saturation pressure (Pa)
H	Height (m)	$S_d$	Water vapour diffusion-equivalent air layer thickness (m)
L	Length (m)	$\mu$	Water vapour resistance factor
t	Time (s)	$A_w$	Capillary absorption coefficient (kg/(m <sup>2</sup> .S <sup>0.5</sup> ))
W <sub>i</sub>	Width (m)	W <sub>lt</sub>	Long-term water absorption by total immersion (volume %)
A	Exposed area of the test specimen (m <sup>2</sup> )	W <sub>f</sub>	Free saturation by total immersion (kg/m <sup>3</sup> )
G	Water vapour flow rate through specimen (kg/s)	V	Volume of the test specimen (m <sup>3</sup> )
S	Hydraulic diameter of specimen (m)	$\rho_w$	Density of water (kg/m <sup>3</sup> )
T	Thermodynamic temperature (K)	$\rho$	Bulk density (kg/m <sup>3</sup> )
$\Delta m_{12}$	Change of mass per time for a single determination with respect to time (kg/s)	c	Specific heat (J/(kg.K))
m <sub>1</sub>	Mass of the test assembly at t <sub>1</sub> (kg)	H <sub>w</sub>	Enthalpy of water (J/m <sup>3</sup> )
m <sub>2</sub>	Mass of the test assembly at t <sub>2</sub> (kg)	$\theta$	Temperature (°C)
m <sub>i</sub>	Initial mass of the specimen (kg)	$\lambda$	Thermal conductivity (W/(m.K))
m <sub>t</sub>	Mass of the specimen at time t (kg)	h <sub>v</sub>	Latent heat of evaporation (J/kg)
t <sub>1</sub> and t <sub>2</sub>	Successive time of weighings (s)	$\varphi$	Relative humidity (%)
G	Mean of five successive determination of $\Delta m_{12}$ for each specimen (kg/s)	w	Moisture content (kg/m <sup>3</sup> )
g	Density of water vapour flow rate(kg/(m <sup>2</sup> s))	D <sub>l</sub>	Liquid diffusivity (m <sup>2</sup> /s)
W	Corrected vapour permeance (kg/(m <sup>2</sup> s Pa))	ACH	Air change per hour (h <sup>-1</sup> )
Z	Water vapour resistance ((m <sup>2</sup> s Pa)/kg)	TWC	Total water content (kg/m <sup>2</sup> )
d	specimen thickness (m)	DR	Dryness rate (%)
da	Thickness of air layer (m)	CR	Condensation Risk (%)
$\delta_a$	Water vapour permeability of air (kg/(m s Pa))	$\phi$	Time lag (h)
		f	Decrement factor
		MGR	Mold growth rate (mm/year)
		MI	Mold index (dimensionless)

also studied carefully for having a primordial role in controlling and regulating indoor relative humidity levels inside the building.

Uncontrolled levels of relative humidity affect indoor air quality, skin humidity, and respiratory comfort, and can also have a significant impact on energy consumption and building envelope degradation [6]. Human thermal comfort, cognitive, and work performance are closely linked to Indoor Environmental Quality (IEQ) [7]. Relative humidities lower than 30 % were associated with an increased risk of respiratory diseases [8]. Damp and high levels of relative humidity (RH) typically above 70–80 % promote an increased risk of mold growth. Exposure to indoor mold contamination has been associated with an increased risk of developing and/or exacerbating a range of allergic and non-allergic diseases [9].

Moreover, Accumulation of moisture in hygroscopic materials can increase their heat conductivity leading to lower energy-saving potential and can cause mold growth and deterioration of artifacts and buildings. Moon et al. [10] found that ignoring moisture transfer contributes to a significant error in the measurement of indoor humidity and an increase in energy consumption by up to 4.4 % energy consumption can be obtained when the effects of moisture are considered.

Currently, building materials for thermal insulation can be primarily categorized into three types based on their origin, chemical substance, and availability: conventional, state-of-the-art, and sustainable [11]. In his research, the author made a comparative analysis of various kinds and performances of building insulation material properties (thermal, hygroscopic, acoustic, reaction to fire, environmental, and cost) in different climate zones and proposed an optimization framework based on energy, environment, economic, and comfort. Moreover, his analysis showed that walls with higher thermal resistance are less cost-effective for regions requiring more cooling and that insulated and airtight houses may also lead to an increased overheating risk during a hot summer.

However, the rising concerns over climate change and the near depletion of non-renewable energy resources have driven the urge for decarbonization of the building sector, the largest energy consumer in

France. In conformity with the EU regulation no 305/2011, the bio-based materials concept was introduced in France in the decree of December 19, 2012, defining the content and the conditions of attribution of the “bio-based building” label. As of the 21st century, bio-insulating materials identified as low-embodied energy materials that reduce energy use and greenhouse gas emissions have experienced relatively recent development in France [12]. For this matter, many researchers have focused on designing and testing various insulation materials made from renewable biomass resources and wastes for building insulation use.

Recent research on natural fiber bio-composites in construction has explored their applications in concrete reinforcement, external strengthening elements, internally filled hollow tubes, wood replacement boards, insulation, and non-structural components. These studies also include life cycle assessments and cost analyses of bio-composites. Research conducted on insulation materials derived from bio-composites has focused on their acoustical, mechanical, and hygrothermal performance, durability, cost, and life cycle assessments. However, most of this research has been conducted at the material scale, with limited studies at the building scale.

In this context, Badouard et al. [13] investigated the development and characterization of new bio-based materials based on viticulture by-products and potato starch for building insulation use. Jerman et al. [14] investigated the hygrothermal properties of five biomaterials (Wood fiberboard, flax fibers, hemp fibers, jute fibers, and sheep wool suitable) potentially applicable in interior thermal insulation systems suitable for historical and traditional buildings. Zhou et al. [15] investigated the influence of fiber size, binder type, and binder ratio on the hygrothermal properties of insulation materials made from rice straw and natural binders.

Moreover, to conduct these investigations, various heat and moisture transfer models have demonstrated notable efficacy in examining the hygrothermal performances of insulation materials. Among them, WUFI® software proved to be a powerful hygrothermal simulation

software based on the model developed by Kunzel [16]. It has complied with the general requirements of standards [17,18] besides being used and experimentally validated over the years by researchers [19–21].

Liuzzi et al. [22] investigated the hygrothermal properties of several clayey materials incorporating different percentages of leaves and small branches derived from the pruning of olive trees. Simon et al. [23] investigated the hygrothermal and mechanical performance of different sustainable concrete mix designs. Coelho et al. [24] validated hygrothermal simulation models for historical buildings while taking into consideration most of the processes that affected the hygrothermal performances.

Nevertheless, the process of hygrothermal performance evaluation involved the study of various risks under different climates for building construction materials (e.g. total water content, drying rate, condensation, mold growth ...). Careful examination of such risks is considered crucial for avoiding any potential damage to building envelope/structure and health hazards.

In this regard, Ho Ryu et al. [25] evaluated the influence of hygric properties of various wallpapers on mold growth rates using hygrothermal simulation. Brambilla and Gasparri [26] investigated condensation and mold growth risk through hygrothermal simulations in timber-based wall assemblies. Tlaji et al. [20] investigated total water content, drying rate, condensation risk, mold growth, moisture quantity, time lag, and decrement factor of various multi-layered straw walls with different boundary conditions. Results showed that the wall's performance strongly depended on the interior and exterior added thermal insulation layers as they affected the ability of the material to dry out. Xue et al. [6] investigated moisture accumulation in building envelopes and its influences on condensation and mold growth. Results showed that moisture content as well as condensation and mold risk are closely related to the building wall orientation.

Furthermore, various researchers investigated a new bio-composite material based on beet pulps derived from the sugar extraction process from sugar beets and potato starch for building insulation use at material and wall scale. Mechanical, hygrothermal, and acoustical studies on this novel material revealed promising results. In this context, Karaky [27] studied during his PhD physical properties (morphology, porosity, density, and particle size), the mechanical, and acoustical performance of starch/Beet pulp bio-composite. A mass ratio equal to 0.4 was found to be the optimal composition of Starch/Beet pulp (S/BP) in terms of hygrothermal and mechanical properties. Costantine et al. [28] compared the drying kinetics and mechanical properties of whole vs. hollowed S/BP bricks having similar mixture composition. Harb et al. [29] studied the thermal performance of S/BP composite for building insulation at a wall scale. Tenpierik et al. [30] Investigated the thermal inertia of S/BP bricks enhanced with phase change materials.

Conducting more room-scale studies can enhance the understanding of bio-composite applications in real projects, addressing the challenges of introducing innovative materials into the well-established construction industry. While there is extensive research on hemp concrete due to its promising results, studies on starch beet pulp have been limited to the material scale. This paper aims to fill these research gaps by extending studies to both the material and room scales, comparing the performance of starch beet pulp to the widely studied hemp concrete, thus providing a better understanding of the bio-composite potential in building applications.

Based on the above findings, this paper aims to elaborate at first thermal and hygric properties of S/BP bio-composite that do not exist in literature. Afterward, an evaluation of the hygrothermal performances and WUFI-Bio mold growth risk assessment for insulation assemblies made of Starch/Beet pulp were conducted using the WUFI® Plus and WUFI®Bio softwares, respectively. This assessment entailed a comparative analysis with insulation assemblies made of hemp concrete, under the climatic conditions of two distinct cities in France - Nancy and Marseille. For this purpose, a renovation case study was adopted for an existing office (6 m × 5 m × 3 m) under Nancy's climate conditions in



Fig. 1. S/BP obtained sample.

France. Insulation walls made of S/BP were attached to the interior of office walls made of clay bricks. Various insulation wall designs were studied.

For each design, the overall energy performance, total water content, drying rate, and condensation risk were evaluated. In the final step, the software WUFI®-Bio was used to evaluate the potential mold risk based on the obtained simulation results from WUFI® Plus software.

## 2. Methodology

### 2.1. Material assembly

In this study, the construction of starch/beet pulp bio-composite was conducted using a similar methodology as described by Costantine et al. [28] while adhering to a mass ratio of 0.4.

This mass ratio has demonstrated its ability to yield optimal results in terms of mechanical, acoustical, and hygrothermal performances [31, 32].

Following the fabrication above procedure, dry extruded beet pulps, with the majority having aggregate lengths and widths varying between 0.5 and 5 mm, and the minority having lengths ranging between 6 and 15 mm, were completely submerged in water with a mass ratio of water to beet pulp set equal to 2.5. This immersion lasted for 2 hours until complete saturation was achieved. Subsequently, manual mixing of potato starch with the saturated wet pulps took place for 10 minutes to ensure thorough homogenization. The mixture was introduced into an autoclave, ensuring a controlled heating at a temperature of 120 °C for 30 minutes. Afterward, Starch/beet pulp samples (L = 21.85 cm, Wi = 10.3 cm, and H = 5.6 cm) were obtained by pouring the mixture into wooden molds and subsequently subjecting it to mechanical compaction at a pressure of 0.044 MPa. In the final step, samples were frozen at -80 °C then dried using a freeze-dryer. The residual moisture content after drying in the lyophilizing chamber was 7 % for a drying time of up to 120 hours.

This drying method resulted in a minimal shrinkage percentage of 2.5 % while maintaining a superior surface quality of the samples compared to pulsed hot air drying. Finally, the obtained samples, as shown in Fig. 1, exhibited a porosity of 70.6 % and a density of 360 kg/m<sup>3</sup>.

### 2.2. Experimental set-up

#### 2.2.1. Determination of water vapor permeability

The water vapor permeability  $\delta_m$  (kg/(m s Pa)) describes the ability of a material to transfer moisture under a gradient of vapor pressure.

During his PhD studies, Karaky [27] performed the "dry cup" test for lower humidities conditions on various Starch-Beet Pulp (S/BP) Composites according to the European standard [33]. Water vapor permeability and water vapor resistance factor were obtained respectively equal to  $6.98 \pm 0.246 \times 10^{-12}$  kg/(m.s.Pa) and  $28.67 \pm 1.02$  for a S/BP composite with a mass ratio of equal to 40 %. In this study, the water



Fig. 2. S/BP samples having their sides sealed with waterproof aluminum tape and fixed at the top of cups enclosing a solution of potassium nitrate (KNO<sub>3</sub>) at their bottoms.

vapor permeability was measured by using the “wet cup” method for higher humidities conditions as described in the same standard.

For this purpose, five cylindrical S/BP samples ( $D = 0.09$  m,  $H = 0.03$  m) were elaborated. They were placed for two weeks inside a climatic chamber Binder MKF 720 conditioned at 50 % RH and 23 °C until mass stabilization.

Afterward, the sides of the specimens were sealed with waterproof aluminum tape, and then each specimen was fixed at the top of a cup enclosing at its bottom a solution of potassium nitrate (KNO<sub>3</sub>) to ensure an inside relative humidity of around  $94 \pm 1$  %. Finally, all specimens were placed inside the climatic chamber Binder MKF 720, as shown in Fig. 2. The air space  $d_a$  (m) between the saturated solution and the specimen was maintained equal to 0.015 m for all tests.

To eliminate the resistance of the air layer above the specimens, an air velocity exceeding 2 m/s was ensured on the top surface of the cups. Cups were regularly weighed by using an analytical balance with 0.001 g resolution every 48 hours until a steady state was reached.

The density of water vapour flow rate  $g$  (kg/(m<sup>2</sup> s)) through a sample was determined by Eqs. (1) and (2):

$$\Delta \dot{m}12 = \frac{m2 - m1}{t2 - t1} \quad (1)$$

$$g = \frac{G}{A} \quad (2)$$

where  $G$  (kg/s) is the mean value of five successive determinations of  $\Delta \dot{m}12$  for each specimen (kg/s) and  $A$ (m<sup>2</sup>) is the Exposed area of the test specimen.

Since the S/BP composite is a highly permeable material based on literature, the resistance of the air gap between the base of the sample and the saturated solution of potassium nitrate (KNO<sub>3</sub>) was considered in the calculation. The corrected vapor permeance  $W$  (kg/(m<sup>2</sup>.s.Pa)) and the water vapor resistance  $Z$  (m<sup>2</sup>.s.Pa)/kg) were determined by Eqs. (3) and (4) respectively and whereas the water vapor pressure difference across specimen  $\Delta p_v$  (Pa) and the Water vapor permeability of air  $\delta_a$  (kg/(m.s.Pa)) were considered equal respectively to 1207 Pa and  $2 \times 10^{-10}$  kg/(m s Pa) for a test condition of 23 °C and 50/93 % RH:

$$W = \frac{1}{\frac{A \cdot \Delta p_v}{G} - \frac{d_a}{\delta_a}} \quad (3)$$

$$Z = \frac{1}{W} \quad (4)$$

Finally, the water vapor permeability of specimen  $\delta$  (kg/(m.s.Pa)), the water vapor resistance factor  $\mu$ , and the water vapor diffusion-

equivalent air layer thickness  $S_d$  (m) were determined respectively by Eqs. (5)–(7):

$$\delta = W \cdot d \quad (5)$$

$$\mu = \frac{\delta_a}{\delta} \quad (6)$$

$$S_d = \mu \cdot d \quad (7)$$

Where  $d$ (m) is the specimen thickness.

#### 2.2.2. Determination of capillary absorption coefficient

The capillary absorption coefficient refers to the capacity of an insulation material to absorb water when only a portion of its surface is exposed for a short time. As a result, the material’s ability to withstand water infiltration into its structure under conditions such as direct exposure to driving rain can be identified.

This coefficient is important for insulation materials, as excessive water absorption can lead to a reduction in their insulating properties and may also cause the material to deteriorate over time. Insulation materials with a low coefficient of water absorption by partial immersion are therefore preferred for applications where moisture resistance is important.

Therefore, the water absorption coefficient value  $A_w$  (kg/(m<sup>2</sup>.s<sup>0.5</sup>)) is thus expressed as the mass of water absorbed by a test specimen per face area  $\Delta m_t$  (kg/m<sup>2</sup>) per square root of time and is determined by a one-directional free water intake test at least for 24 h according to the European standard NF EN ISO 15148 as described by Eqs. (8) and (9):

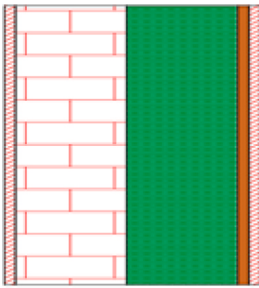
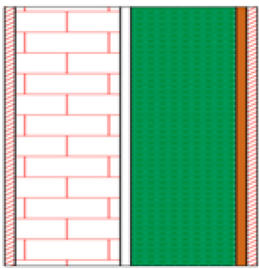
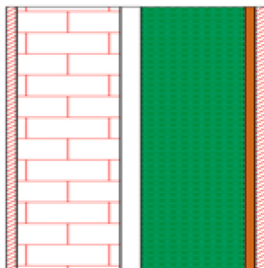
$$\Delta m_t = \frac{m_t - m_i}{A} \quad (8)$$

$$A_w = \frac{\Delta m_t}{\sqrt{t}} \quad (9)$$

For this purpose, four identical S/BP bricks ( $L = 0.2185$  m,  $W_i = 0.103$  m and  $H = 0.056$  m) were elaborated. Bricks were placed for two weeks inside a climatic chamber Binder MKF 720 conditioned at 50 % RH and 23 °C. After mass stabilization, each brick was weighed with a balance capable of weighing test specimens to an accuracy of  $\pm 0.1$  % to determine their initial weights  $m_i$ . The sides of the bricks were sealed with waterproof aluminum tape to ensure one-dimensional water flow.

Then they were placed inside a tank on point supports to keep it clear from the bottom. The tank was partially filled with water conditioned at 23 °C until it reached 5 mm higher than the submerged base of the specimen placed inside the tank. The water level was maintained at this

**Table 1**  
Different insulation wall assemblies of five considered cases.

Case	Wall assembly design					
	Layer 1	Layer 2	Layer 3	Layer 4	Layer 5	Layer 6
(0) 	Exterior plaster (2 cm)	Clay brick (20 cm)	Interior plaster (2 cm)	-	-	-
(a) 	Exterior plaster (2 cm)	Clay brick (20 cm)	S/BP (10 cm)	Hardwood (2 cm)	Interior plaster (2 cm)	-
(b) 	Exterior plaster (2 cm)	Clay brick (20 cm)	S/BP (20 cm)	Hardwood (2 cm)	Interior plaster (2 cm)	-
(c) 	Exterior plaster (2 cm)	Clay brick (20 cm)	Non-ventilated air layer (2 cm)	S/BP (20 cm)	Hardwood (2 cm)	Interior plaster (2 cm)
(d) 	Exterior plaster (2 cm)	Clay brick (20 cm)	Non-ventilated air layer (4 cm)	S/BP (20 cm)	Hardwood (2 cm)	Interior plaster (2 cm)

level ± 2 mm during all the tests. Each brick was weighted after 1,3,5,7,10,15,20,30,60,120,1440 minutes.

**2.2.3. Determination of moisture content at free saturation**

The moisture content at free saturation for insulation materials refers

to the highest amount of water that a material can freely absorb when submerged in water for a long time without a vacuum. It is defined in literature by the long-term water absorption by total immersion coefficient Wlt (volume percent) or by the free water saturation coefficient Wf (kg/m3).

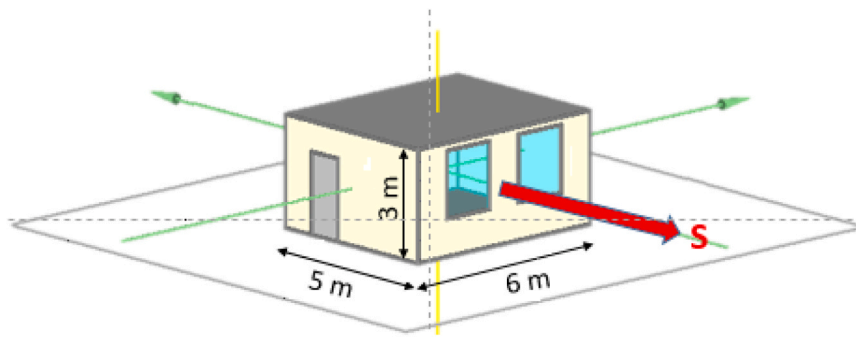


Fig. 3. Schematic representation of the office under investigation.

For bio-composite materials,  $W_{lt}$  depends on various factors such as the type and amount of natural fibers used, the type of binder, and the manufacturing process. The determination of this coefficient is inevitable for bio-composites materials as water saturation can compromise the insulating properties' effectiveness and potentially affect the mechanical properties by weakening the natural fibers and leading to dimensional changes or even structural damage.

In this study,  $W_{lt}$  was determined in a free water intake test by totally immersing S/BP bricks in water according to Method 2 A (long-term water absorption by total immersion - drainage) listed in the European standard [34].

For this purpose, four identical S/BP bricks ( $L = 0.2185$  m,  $W_i = 0.103$  m, and  $H = 0.056$  m) were elaborated and were placed for two weeks inside a climatic chamber Binder MKF 720 conditioned at 50 % RH and 23 °C.

Afterward, each brick was placed inside an empty tank. A sufficient point load was applied to it to keep the tested specimen immersed in water while maintaining the slightest contact possible with the load.

In a later step, the tank was filled with water conditioned at 23 °C until the top face of the test specimen ( $50 \pm 2$  mm) was submerged below the surface of the water. The water level was maintained at this level during all the test.

Long-term water absorption by total immersion  $W_{lt}$  (%) and  $W_f$  ( $\text{kg}/\text{m}^3$ ) was determined based on the total water absorbed after saturation

by Eqs. (10) and (11) respectively:

$$W_{lt} = \frac{m_t - m_i}{V} \times \frac{100}{\rho_w} \tag{10}$$

$$W_f = \frac{m_t - m_i}{V} \tag{11}$$

Where  $V$  ( $\text{m}^3$ ) is the volume of the test specimen and  $\rho_w$  ( $\text{kg}/\text{m}^3$ ) is the density of water.

#### 2.2.4. Determination of thermal conductivity

In their study, Karaky [32] examined the thermal conductivity of S/BP at an ambient temperature of 20 °C and a relative humidity of 10 %. Under these specific conditions, the thermal conductivity of this bio-composite for a mass ratio equal to 0.4 was determined equal to 0.0757  $\text{W}/(\text{m} \cdot \text{K})$ .

To further investigate the correlation between thermal conductivity and relative humidity, thermal conductivity tests were carried out on three identical S/BP bricks ( $L = 0.1$  m,  $W_i = 0.1$  m, and  $H = 0.1$  m) regulated for two weeks at an ambient temperature of 20 °C and a relative humidity of 60 %. The thermal conductivities were measured using an Isomet 2114 (Applied Precision) device, which employs a dynamic measurement method to reduce the measurement time in comparison with steady state measurement methods. The heat flow is

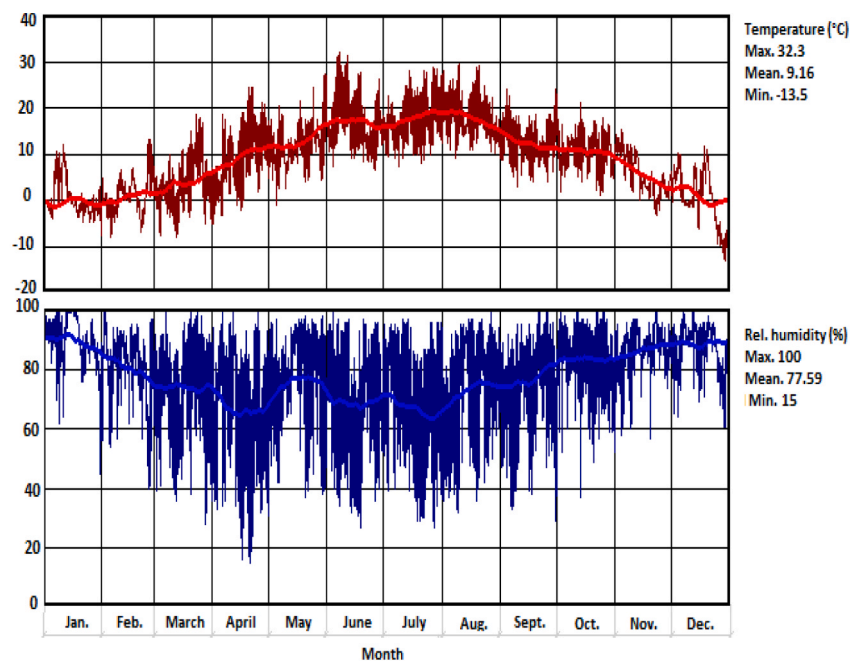


Fig. 4. Outer temperature and relative humidity information obtained from WUFI®Plus for Nancy's climate.

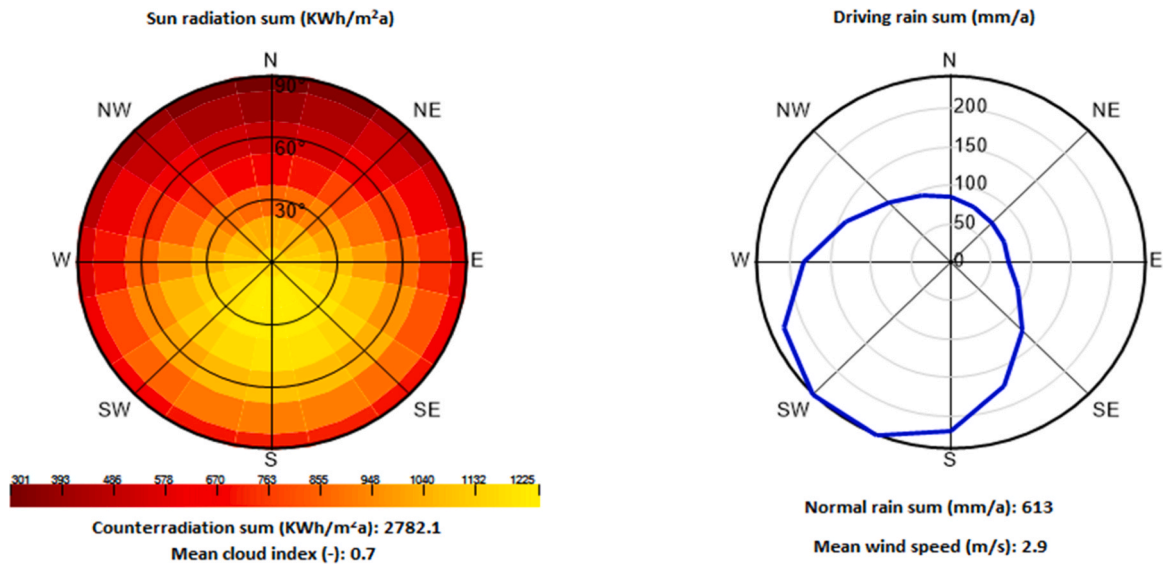


Fig. 5. Sun radiation and driving rain information obtained from WUFI®Plus for Nancy's climate.

produced by an electrical heating of resistor heating in direct contact with the tested sample. The assessment of thermal conductivity is performed by periodically recording the sampled temperature as a function of the time. The measurement reproducibility of the device was 3 % + 0.001 W/(m.K).

### 3. Numerical simulation

#### 3.1. Methodology overview

It is important to note that the S/Bp bio-composite material is not intended for use as a structural building material, and should not be exposed to very high levels of humidity under normal use. Rather, It is designed to be installed as interior insulation within the building envelope.

For this study, hygrothermal studies and mold growth risk assessment were conducted to examine four different insulation assemblies made of S/BP, as described in Table 1. These investigations aimed to assess the effects of increasing the thickness of bio-composite insulation materials and incorporating various stationary air layers on humidity ingress, energy consumption, and potential health hazards affecting the overall performance of a building. To evaluate the hygrothermal performances and mold growth risk assessment of these assemblies, a simplified one-story office building (6 m x 5 m x 3 m) was modeled in WUFI® Plus as shown in Fig. 3. This software showed to be the most complete heat and moisture simulation tool in the WUFI® software family. In addition to simulating hygrothermal conditions of different building components, it is suitable for addressing energy consumption and comfort in buildings. Consequently, poor performance and/or damage can be avoided in the building design phase (e.g., summer

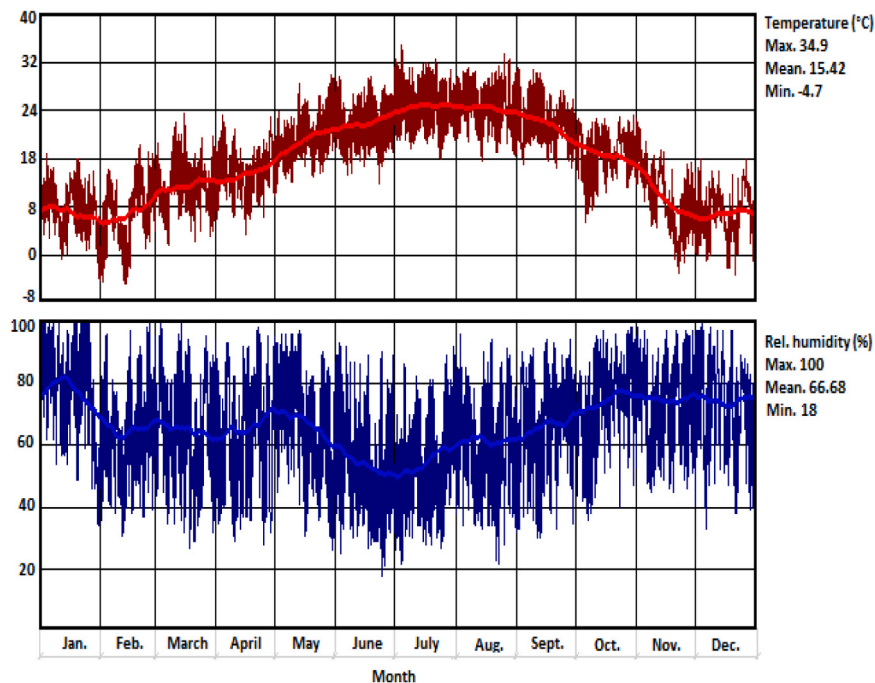


Fig. 6. Outer temperature and relative humidity information obtained from WUFI®Plus for Marseille's climate.



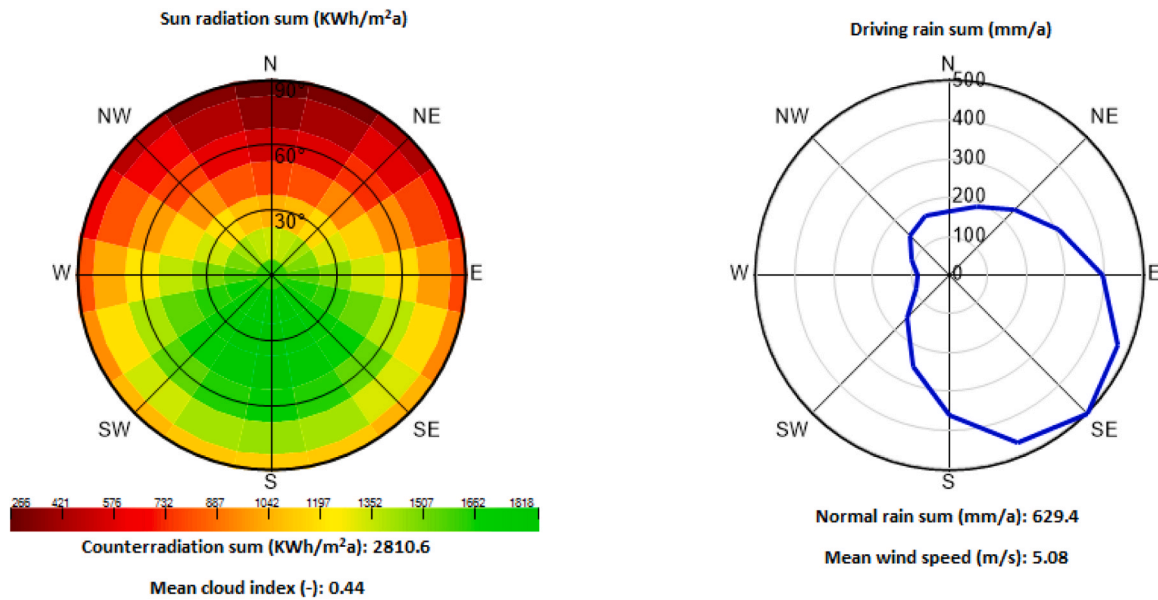


Fig. 7. Sun radiation and driving rain information obtained from WUFI®Plus for Marseille's climate.

overheating, mold, etc. ...) [35].

The purpose of this simulation is to evaluate the viability of these assemblies as internal insulation for office walls constructed with aerated clay brick, under two distinct climatic conditions in France, namely the cities of Nancy and Marseille which experience vastly different weather patterns. Subsequently, a comparative performance analysis is made between the S/BP bio-composite and hemp concrete for the four different assemblies used in this study under Nancy's climate. Given the extensive study on hemp concrete in literature, its material setup was unnecessary, and all required hygrothermal performance data for this study were obtained from existing literature sources [36] [37].

For each case, the overall energy performance, total water content, drying rate, condensation risk, mold growth, time lag, and decrement factor were evaluated through numerical simulations.

The outer temperature and relative humidity, sun radiation, and driving rain information for the French cities of Nancy and Marseille were acquired from the built-in database within the WUFI® Plus program and are shown in Figs. 4–7 respectively.

A numerical model based on WUFI®Plus software is used to predict the hygrothermal response of the S/BP wall assemblies under different weather conditions. It was developed by the Fraunhofer Institute for Building Physics (Germany) and is based on solving the coupled heat and moisture transfer models proposed by Künzle [16] as shown in Eqs. (12) and (13):

$$\left( \rho c + \frac{\partial Hw}{\partial \theta} \right) \cdot \frac{\partial \theta}{\partial t} = \nabla \cdot (\lambda \Delta \theta) + hv \nabla \cdot (\delta p \nabla (\phi P_{sat})) \quad (12)$$

$$\frac{\partial w}{\partial \phi} \cdot \frac{\partial \phi}{\partial t} = \nabla \cdot (Dl \cdot \frac{\partial w}{\partial \phi} \nabla \phi) + \delta p \nabla (\phi P_{sat}) \quad (13)$$

where  $\rho$ ,  $c$  are respectively the bulk density ( $\text{kg/m}^3$ ) and the specific heat ( $\text{J}/(\text{kg}\cdot\text{K})$ ) of the dry material and  $Hw$ ,  $\theta$ ,  $t$ ,  $\lambda$ ,  $h$ ,  $v$ ,  $\delta p$ ,  $\phi$ ,  $P_{sat}$ ,  $w$  and  $Dl$  are respectively the enthalpy of water ( $\text{J}/\text{m}^3$ ), the temperature ( $^{\circ}\text{C}$ ), the time (s), the thermal conductivity ( $\text{W}/(\text{m}\cdot\text{K})$ ), the latent heat of evaporation ( $\text{J}/\text{kg}$ ), the vapor permeability ( $\text{kg}/(\text{m}\cdot\text{s}\cdot\text{Pa})$ ), the relative humidity, the saturation vapor pressure (Pa), the moisture content ( $\text{kg}/\text{m}^3$ ) and the liquid diffusivity ( $\text{m}^2/\text{s}$ ).

The primary mechanism for moisture transport mechanism in capillary porous materials is capillary liquid transport. This mode of transport can be characterized by two distinct liquid transport coefficients: The liquid transport coefficient for suction  $D_{ws}$  ( $\text{m}^2/\text{s}$ ) and

Table 2

Basic data of uncoated double glazing window acquired from the built-in database within WUFI®Plus software.

Uw-mounted ( $\text{W}/(\text{m}^2\cdot\text{K})$ )	2.73
Frame factor	0.7
Solar Energy transmittance hemispherical	0.6
Long wave radiation emissivity (mean glazing/frame)	0.85
Total solar transmission for a solar radiation angle equal to $0^{\circ}$	0.7
Total solar transmission for a solar radiation angle equal to $60^{\circ}$	0.58
Total solar transmission for a solar radiation angle equal to $90^{\circ}$	0.23

the liquid transport coefficient for redistribution  $D_{ww}$  ( $\text{m}^2/\text{s}$ ).

The  $D_{ws}$  describes the capillary uptake of water by a building facade during exposure to rainfall, wherein the transport is dominated by the larger capillaries. In contrast,  $D_{ww}$  describes the dispersion of absorbed water within the materials after the rain has ceased, with transport dominated by the smaller capillaries.

Unfortunately, the aforementioned transport coefficients are difficult to measure for the majority of materials. Reliant on the water content, the liquid transport coefficient for suction  $D_{ws}$  ( $\text{m}^2/\text{s}$ ) and the liquid transport coefficient for redistribution  $D_{ww}$  ( $\text{m}^2/\text{s}$ ) can be estimated by using WUFI®Plus software as shown in Eqs. (14)–(16):

$$D_{ws}(w) = 3.8 \cdot \left( \frac{Aw}{wf} \right)^2 \cdot 1000 \left( \frac{w}{wf} \right)^{-1} \quad (14)$$

$$D_{ww}(w80) = D_{ws}(w80) \quad (15)$$

$$D_{ww}(wf) = D_{ws}(wf)/10 \quad (16)$$

Where  $w$  ( $\text{kg}/\text{m}^3$ ) is the moisture content mass by volume,  $w80$  and  $wf$  indicate a moisture content for a relative humidity equal to 80 % and 100 % respectively.

### 3.2. Materials and design conditions

Based on the literature, a duration of 4 years was deemed efficient for conducting hygrothermal studies. Consequently, each hygrothermal study was carried out over four years, with results recorded at one-hour intervals. The calculation accuracy was set to very high. The following design conditions were consistently held constant for all simulations:

At the southern façade, two uncoated double-glazed windows were

**Table 3**

Metabolic rate data for one adult/sitting person/working acquired from the built-in database within WUFI®Plus software.

Setting	Heat convective (W)	Heat radiant (W)	Moisture (g/h)	CO2 (g/h)	Human activity (met)
Adult, sitting person, working	80	41	59	36.3	1.2

installed, each measuring 1.5 m in width and 1.8 m in height. The basic data for these windows are provided in Table 2.

Consequently, the ratio of window area per floor area reached 18 %. Additionally, on the Western façade, a wooden door measuring 1 m in width and 2.2 m in height was incorporated into the structure.

Given the specific focus of the hygrothermal analysis on evaluating the impact of insulation assemblies on wall components and the overall performance of the system, an assumption was made that the slab and roof experienced no heat or moisture exchange with the external climate. Consequently, both components were treated as adiabatic and impermeable materials.

Moreover, because the hygrothermal behaviour of a wall is significantly affected by various factors such as solar radiation, driving rain intensity and direction as well as the orientation of the structure, the focus is made on north-oriented walls, as this orientation tends to experience higher driving rain intensity and lower solar radiation which amplifies the likelihood of encountering moisture-related issues.

It is assumed that the office building is occupied from 08:00–17:00, five days per week with 3 adults working in an office job.

Within the designated occupancy hours, the metabolic rates generated by each individual are listed in Table 3, acquired from the built-in database within WUFI®Plus software. Moreover, an additional internal load of 200 Watts was presumed for other internal loads originating from lighting fixtures and various office equipment.

To ensure the maintenance of a comfortable and healthy indoor environment, a mechanical ventilation system was established in conjunction with permanent air infiltration through building leakages. The air change per hour ACH ( $\text{h}^{-1}$ ) values were set equal to 1.5 and 0.1 for mechanical ventilation and air infiltration, respectively.

Only temperature was controlled for all designs through a heating and a cooling systems. Temperature set points were established at 21 °C and 25 °C.

Conversely, during non-occupancy hours, no internal loads were generated, and the ACH for the mechanical ventilation system was consistently maintained at a value of 0.75. Furthermore, the maximum and minimum temperature set-point values for the cooling and heating systems were set equal to 17 °C and 27 °C, respectively.

Lastly, the hygrothermal characteristics of the building materials

**Table 4**

Building materials hygrothermal properties.

Element	$\rho$ ( $\text{kg}/\text{m}^3$ )	Porosity (-)	$C_p$ (J/(kg. K))	$\lambda$ , dry 10 °C (W/(m. K))	$\mu$ , dry (-)	$W_f$ ( $\text{kg}/\text{m}^3$ )	$A_w$ ( $\text{kg}/(\text{m}^2. \text{s}^0.5)$ )	References
Exterior plaster	1310	0.36	850	0.87	8	192	0.001	The database of WUFI®Plus software
Aerated clay brick	672	0.67	850	0.12	4	291	0.046	The database of WUFI®Plus software
Air layer (2 cm)	1.3	0.999	1000	0.13	0.56	-	-	The database of WUFI®Plus software
Air layer (4 cm)	1.3	0.999	1000	0.23	0.38	-	-	The database of WUFI®Plus software
S/BP	360	0.706	1410	0.075	28.67	641.59	0.154	This study; Karaky [27]
Hardwood	650	0.47	1400	0.13	200	-	-	The database of WUFI®Plus software
Interior plaster	850	0.65	850	0.2	8.3	400	0.287	The database of WUFI®Plus software
Hemp concrete	466	0.78	741	0.0995	2.02	541	0.14	Seng et al., [36,37]

used in this study are listed in Table 4, while Table 5 presents the moisture storage functions for HC and S/BP.

### 3.3. WUFI Plus-hygrothermal simulation

The impact of each configuration was assessed by evaluating the overall cooling load during summer and, heating load during winter.

Excessive moisture content in building materials can lead to various detrimental effects such as decreased thermal performance, bio-degradation, mold growth, and structural decay. Using WUFI®Plus software, detailed predictions were made for the total water content, drying rate, and condensation risk criteria. Based on the findings, moisture concerns were identified and highlighted for each configuration.

The total water content TWC refers to the amount of water present within a building material at a specific time for specific environmental conditions. A day average of the total water content is estimated by the WUFI®Plus software for all scenarios over four years. The variations in the total water content observed throughout these years will indicate whether the material will encounter excessive moisture content or maintain a stable state. This evaluation can be conducted by comparing the initial and the final moisture content. The criterion for passing this assessment is met if the final water content is lower than its initial content.

The dryness rate measures the ability of a wall to dry out and reduce its moisture content. For each configuration, it is equal to the difference between the total initial water content  $TWC_i$  ( $\text{kg}/\text{m}^2$ ) and the total final water content  $TWC_f$  ( $\text{kg}/\text{m}^2$ ) of all layers within the studied assembly divided by its total initial water content over four years as shown in Eq. (17):

$$DR = \frac{TWC_i - TWC_f}{TWC_i} \times 100 \quad (17)$$

A negative rate of DR signifies that the wall is accumulating humidity and moisture throughout the study period, rendering it highly susceptible to moisture-related issues. Conversely, a positive rate indicates that

**Table 5**

Moisture storage function comparison between HC and S/BP.

	RH (%)					References
	20	40	60	80	92	
Water content within HC ( $\text{kg}/\text{m}^3$ )	5.65	8.71	12.68	20.32	29.96	Karaky [27]
Water content within S/BP ( $\text{kg}/\text{m}^3$ )	6.16	17.26	31.32	53.02	67.56	Seng et al. [36,37]

the wall is progressively shredding the humidity. Whereas, higher values of DR reflect a greater ability to eliminate moisture, while lower values indicate a slower rate of moisture reduction.

Subsequently, monitoring the DR is crucial for understanding the overall moisture performance and durability of the building envelope.

Condensation risk (CR) refers to the potential for water vapor to condensate within the building envelope. This risk can manifest either on the indoor surface or within the wall. Surface condensation occurs when its temperature falls below the dew point temperature within the indoor environment. In such cases, The CR is determined by calculating the percentage of time the surface temperature remains below the dew point.

Within the wall, CR arises when the vapor pressure exceeds the saturated vapor pressure. In this study, the risk was evaluated based on the ASHRAE standard 160 P, which prescribes the criteria for moisture control design and analysis in buildings [38]. This standard, which was also employed by Brambilla and Gasparri [26], sets three performance criteria aimed at minimizing potential issues related to moisture and mold growth within the building envelope, in particular:

- A. 30-day running average surface relative humidity to be lower than 80 %
- B. 7-day running average surface relative humidity to be lower than 98 %
- C. 24-hour running average surface relative humidity to be lower than 100 %

Subsequently, The CR within the wall is determined by quantifying the percentage of time during which these criteria were not met.

To gain a deeper understanding of the dynamic thermal behaviour of the various insulation assemblies, an investigation was made to determine their ability to maintain thermal comfort and energy efficiency under various factors, including daily temperature fluctuations and climatic conditions. Consequently, a comparative analysis was conducted on the time lag parameter and the decrement factor for each insulation assembly.

The time lag refers to the duration that a heatwave requires to cross through an assembly from one surface to another. In another word it represents the delay between the peak of a temperature on one surface and the corresponding temperature peak response on the opposing surface. A longer time lag indicates a slower heat transfer through a material.

Whereas, the decrement factor refers to the rate of attenuation in the amplitude of a heatwave as it propagates through an assembly. A higher decrement factor reflects a higher capacity of a material in dampening heat transfer.

The time lag  $\phi$  (h) and decrement factor  $f$  (-) can be obtained as shown in Eqs. (18) and (19) respectively [39]:

$$\phi = tint, \max - text, \max \tag{18}$$

$$f = \frac{Tint, \max - Tint, \min}{Text, \max - Text, \min} \tag{19}$$




Where  $tint, \max$  and  $text, \max$  represent the time when interior and exterior temperatures reach their respective peak values. Additionally,  $Tint, \max$ ,  $Tint, \min$ ,  $Text, \max$  and  $Text, \min$  represent the maximum and minimum temperatures attained by the internal and external surfaces, respectively.

### 3.4. Wufi-Bio mold growth risk assessment

Based on the hygrothermal simulation results for the studied insulation assemblies obtained from the WUFI®Plus software, mold growth risk assessment were conducted through WUFI-Bio mold growth risk assessment simulations. This assessment was carried out utilizing the WUFI®Bio software, which is widely used in literature for predicting the growth of mold and fungi growth building materials [25,40].

**Table 6**

General assessment of the mold growth risk and the severity of the infestation acquired from the built-in database within WUFI®Plus software.

Signal light		Surfaces inside constructions without direct contact to indoor air
	Mold Growth Mold Index Assessment	< 176 mm/year $\leq 2$ Usually acceptable
	Mold Growth Mold Index Assessment	176 < MGR $\leq$ 239 mm/year $2 < MI \leq 3$ Additional criteria or investigations are needed for assessing acceptability
	Mold Growth Mold Index Assessment	> 239 mm/year, >3 Usually not acceptable

**Table 7**

Mold index description acquired from the built-in database within WUFI®Plus software.

Mold Index	Description
0	no growth
1	some growth visible under microscope
2	moderate growth visible under microscope, coverage more than 10 %
3	some growth detected visually, thin hyphae found under a microscope
4	visual coverage of more than 10 %
5	coverage more than 50 %
6	tight coverage, 100 %

Based on the decisive parameters affecting mold growth, namely temperature, relative humidity, and substrate quality, the WUFI®Bio software generates the germination isopleth graphs. During each time step, with the changing ambient temperature and humidity, this software computes the transient water content within a spore of a material and compare it to the critical water content obtained from the moisture storage function of the material.

The WUFI®Bio software assumes that germination occurs and mycelium growth initiates when the water content in the model spore exceeds the critical water content. Once germination is established, the mycelium growth isopleth system is used to estimate the extent of growth. However, growth is assumed to be stopped when the water content in the spore falls below the critical water content. Nevertheless, it resumes growing instantly when the critical water content is exceeded again.

It is to be noted that the WUFI®Bio software does not incorporate biogenic factors, pH value, surface quality, and several other influential factors that can potentially hinder the process of germination and growth. Thus, the simulation results tend to be conservative, indicating a higher risk of mold growth compared to real conditions. In this study, the S/BP and hemp concrete materials used are treated as surfaces within constructions without direct contact to indoor air. Moreover, they are presumed to belong to substrate class I, denoting bio-utilizable substrates. Risk levels of each assembly were assessed based on the mold growth rate MGR (mm/year) measured on a yearly basis reflecting the expected mycelium growth (in mm) after germination, mold index MI (-) describing the mold-infested fraction of a surface of material and a signal light summarizing the mold growth risk indicated by WUFI®Bio

**Table 8**

Water vapour permeability  $\delta$  (kg/(m.s.Pa)) and water vapor resistance factor  $\mu$  comparison of S/BP composite for lower and higher humidities conditions.

$\delta$ value x E-11(kg/(m.s.Pa))		$\mu$ Value (-)					
"dry cup"	Reference	"wet cup"	Reference	"dry cup"	Reference	"wet cup"	Reference
$6.98 \times 10^{-12} \pm 0.25 \times 10^{-12}$	Karaky [27]	$5.82 \times 10^{-11} \pm 4.8 \times 10^{-12}$	This study	$28.67 \pm 1.02$	Karaky [27]	$3.45 \pm 0.3$	This study

**Table 9**

Water vapour resistance factor  $\mu$  at higher humidities conditions for S/BP composite and other biomaterials suitable for thermal insulation.

Material	$\mu$ Value (-)	References
S/BP	$3.45 \pm 0.3$	This study
Hemp concrete	1.43	Seng et al. [36,37]
Various Hemp bio-insulation materials	30 % Hemp fiber, 60 % wood fiber, 10 % polyester	Latif et al. [41]
	85 % Hemp fibers, 10–12 % bicomponent fibers and 3–5 % soda	
	70 % Hemp fibers, 15 % hemp shive, 8 % ammonium phosphate, 7 % polyolefin fibers	
	95 % Hemp fibers and 5 % combination recycled adhesive binder	
	35 % Hemp fiber, 35 % recovered waste cotton fiber, 15 % bi-component polyester fiber and 15 % fire retardant	
Wood fiberboard	$1.12 \pm 0.28$	Jerman et al.. [14]
flax fibers	$1.03 \pm 0.28$	
hemp fibers	$1.46 \pm 0.62$	
jute fibers	$1.23 \pm 0.31$	
sheep wool	$1.62 \pm 0.62$	

software in a simple 'yes/maybe/no' acceptability scheme. Lastly, the general assessment of the mold growth risk and mold index description are listed in Tables 6 and 7, respectively.

## 4. Results and discussions

### 4.1. Experimental findings

#### 4.1.1. Water vapor permeability

The results of water vapor permeability and water vapor resistance factor for the S/BP composite under elevated humidity conditions, determined using the "wet cup" method are presented in Table 8.

It is evident that the water vapor resistance factor  $\mu$ , as determined through the "dry cup" method for the S/BP composite, exhibits a higher value compared to its corresponding value obtained by the "wet cup" test method for the same composite. Moreover, the obtained water vapor resistance factor  $\mu = 3.45$  at higher humidities conditions for S/BP composite is slightly higher than the water vapor resistance at higher humidities conditions of other biomaterials suitable for building insulation listed in Table 9. This is credited to the small size of the beet pulps (2–4 mm) and to the high mass ratio of starch/BP equal to 40 %, which provides a more homogenous and less porous composite than the others. Finally, the analyzed S/BP composite exhibited a relatively low water vapour resistance factor  $\mu$ , rendering it well-suited for humidity moderation.

#### 4.1.2. Capillary absorption coefficient

For each brick, the mass of water absorbed by per face area  $\Delta mt$  (kg/m<sup>2</sup>) was plotted as a function of the square root of time as shown in Fig. 8.

It can be observed that the curves are not linear but rather exhibit various non-linear forms and thus were considered as type B according to European standard [42]. Consequently, the capillary absorption coefficient (kg/(m<sup>2</sup>.S<sup>0.5</sup>)) through partial immersion was determined based on the water absorbed after 24 hours, as shown in Eq. (20):

$$Aw, 24 = \frac{\Delta mtf}{\sqrt{86400}} \tag{20}$$

It was observed that prolonged exposure to liquid water has led to alterations in the surface structure of the S/BP insulation brick in contact with water, with a noticeable increase in density near the surface.

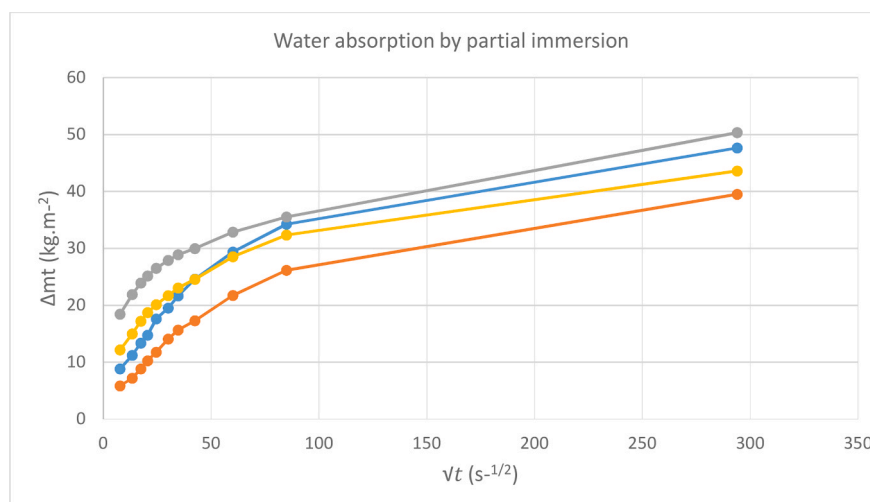


**Fig. 8.** Measurements of the water absorption coefficient by partial immersion of the S/BP bricks.

**Table 10**

Water absorption coefficient by partial immersion  $A_w$  for S/BP composite and other biomaterials suitable for thermal insulation.

Material	$A_w$	References	
S/BP	$0.154 \pm 0.016$	This study	
hemp concrete	$0.14 \pm 0.01$	Seng et al. [36,37]	
Various Hemp bio-insulation materials	30 % Hemp fiber, 60 % wood fiber, 10 % polyester 17	0.041	Latif et al. [41]
	85 % Hemp fibers, 10–12 % bicomponent fibers, and 3–5 % soda	0.034	
	70 % Hemp fibers, 15 % hemp shive, 8 % ammonium phosphate, 7 % polyolefin fibers	0.033	
	95 % Hemp fibers and 5 % combination recycled adhesive binder	0.029	
	35 % Hemp fiber, 35 % recovered waste cotton fiber, 15 % bi-component polyester fiber, and 15 % fire retardant	0.031	
Wood fiberboard	$0.18 \pm 0.03$	Jerman et al. [14]	
flax fibers	$0.35 \pm 0.08$		
jute fibers	$0.52 \pm 0.1$		
sheep wool	$0.14 \pm 0.03$		

Consequently, the S/BP composite was deemed unsuitable for external insulation purposes. The average values obtained for the capillary absorption coefficient by partial immersion  $A_w$  of the S/BP composite were found equal to  $0.154 \pm 0.016 \text{ kg}/(\text{m}^2 \cdot \text{s}^{0.5})$ . This value, as presented in Table 10, was observed to be greater than  $A_w$  values for hemp concrete (Seng et al., 2019) and other various hemp-bio insulation materials [41], while being lower than  $A_w$  values for Wood fibreboard, flax fibers, jute fibers [14].

#### 4.1.3. Moisture content at free saturation

Owing to the important hydrophilic character of Beet Pulps by having their pores easily accessible and quickly filled with water leading to material swelling [43], test specimens were weighed after 24 and 96 h.

A rapid increase in the mass of the S/BP bricks was observed after the first hours of immersion in water while a relatively minor change was observed after 24 h. Therefore, the test was stopped after 96 h of immersion to avoid structural damage to the tested bricks. The density of water was assumed to be  $1000 \text{ kg}/\text{m}^3$  and the obtained results for  $W_t$  and  $W_f$  for S/BP bio composites bricks were respectively equal to  $64.16 \pm 3.74 \text{ vol}\%$  and  $641.59 \pm 37.43 \text{ kg}/\text{m}^3$ .

**Table 11**

Energy consumption analysis of various insulation assemblies with S/BP or HC under Nancy's and Marseille's climates.

Conf.	Case	Under Nancy's climate				Under Marseille's climate			
		Heating Load (kWh)	Cooling Load (kWh)	Annual Total Load (kWh)	Reduction in total energy consumption (%)	Heating Load (kWh)	Cooling Load (kWh)	Annual Total Load (kWh)	Reduction in total energy consumption (%)
Primary	(0)	3104	334	3437	-	981	1421	2402	-
Insulation material based on Hemp concrete	(a)	2262	398	2660	22.6 %	614	1284	1898	21.0 %
	(b)	1845	455	2301	33.1 %	430	1384	1814	24.5 %
	(c)	1796	464	2260	34.3 %	409	1398	1807	24.8 %
	(d)	1765	470	2236	35.0 %	397	1408	1804	24.9 %
Insulation material based on Starch/ Beet pulp	(a)	2152	413	2566	25.4 %	556	1308	1864	22.4 %
	(b)	1730	472	2201	36.0 %	372	1406	1778	26.0 %
	(c)	1678	482	2160	37.2 %	351	1427	1777	26.0 %
	(d)	1663	485	2148	37.5 %	345	1432	1777	26.0 %

#### 4.1.4. Thermal conductivity

The thermal conductivity tests carried out on the S/BP bio-composite having a mass ratio equal to 0.4 at an ambient temperature of  $20^\circ\text{C}$  and a relative humidity of 60 % yielded a thermal conductivity equal to  $0.108 \pm 0.0193 \text{ W}/(\text{m K})$ . This value exceeded the thermal conductivity observed for the same material at an ambient temperature of  $20^\circ\text{C}$  and a relative humidity of 10 % which was determined to be equal to  $0.0757 \text{ W}/(\text{m K})$  [32].

Therefore, the increase in relative humidity levels leads to a reduction in the insulation effectiveness of the S/BP bio-composite which can be attributed to its hydrophilic nature. As relative humidity levels increase, the material's capacity to absorb water increases. The absorbed water molecules displace the air within the pores which will lead to a more efficient heat conduction inside the material as water exhibits higher thermal conductivities compared to air. Moreover, the presence of these water molecules can also exert an influence on the material fibers' properties as they may experience swelling or even changes in their physical structure, further contributing to the evolving thermal characteristics of the studied S/BP composite.

## 4.2. Numerical simulation

### 4.2.1. Hygrothermal simulation

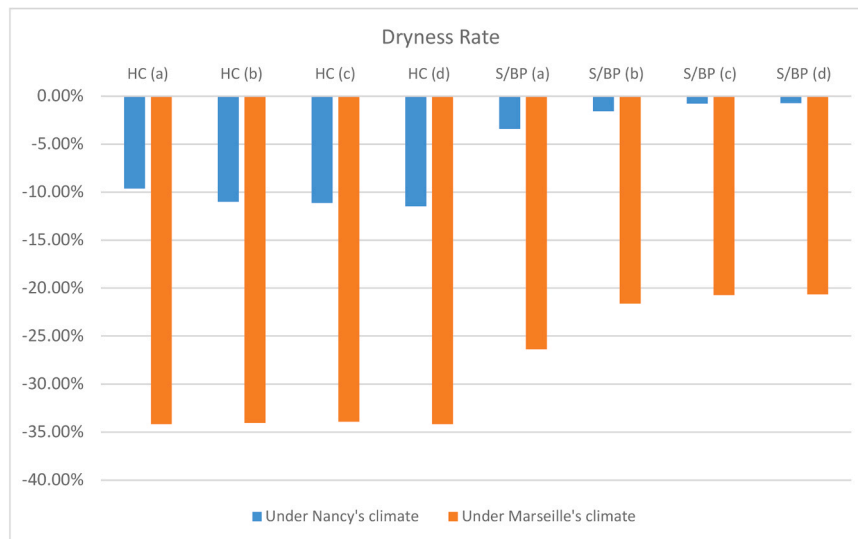
**4.2.1.1. Energy performance.** An energy performance analysis detailing the required cooling and heating loads was conducted on each insulation assembly. The findings were subsequently compared with the energy consumption of the baseline configuration under Nancy's and Marseille's climates. The outcomes of these studies are outlined in Table 11.

Table 11 shows that for Nancy's climate, heating demand exceeds the cooling one whereas for Marseille it is the opposite. This was expected given that Nancy's climate having a mean temperature equal to  $9.16^\circ\text{C}$  is colder than Marseille's climate with a mean temperature equal to  $15.42^\circ\text{C}$ , as shown in Figs. 4 and 6 respectively. The total annual energy demand for the primary scenario (case 0) within Nancy's climatic conditions was determined to be 3437 kWh, 43.1 % higher compared to the corresponding total annual energy demand under Marseille's climatic conditions.

The incorporation of bio-insulation materials in accordance with case (a), resulted in a slight increase in annual cooling demand but a more substantial reduction in heating demand, leading to a decrease in total required annual energy consumption to 2660 kWh and 1898 kWh for HC and to 2566 kWh and 1864 kWh for S/BP under Nancy's and Marseille's climates, respectively. Hence, a reduction in total energy consumption relative to case (0) was achieved equal to 22.6 % and 21 % for HC and 25.4 % and 22.4 % under the two studied climates, respectively. A further reduction in total energy consumption was achieved when increasing the thickness of bio-insulation materials from 10 cm to 20 cm in accordance with case (b) where it reached 2301 kWh and 1814

**Table 12**  
Total water content (kg/m<sup>2</sup>) analysis of insulation assemblies with S/BP or HC under Nancy's and Marseille's climates.

Config.	Case	Under Nancy's climate					Under Marseille's climate				
		TWC i	TWC 1	TWC 2	TWC 3	TWC f	TWC i	TWC 1	TWC 2	TWC 3	TWC f
Insulation material based on Hemp concrete	(a)	10.02	10.83	10.95	11.00	10.98	10.02	12.85	13.32	13.42	13.44
	(b)	12.05	13.14	13.31	13.38	13.38	12.05	15.24	15.93	16.11	16.15
	(c)	12.05	13.16	13.33	13.40	13.39	12.05	15.24	15.92	16.10	16.14
	(d)	12.05	13.19	13.37	13.44	13.43	12.05	15.26	15.95	16.13	16.17
Insulation material based on Starch/Beet pulp	(a)	13.31	13.82	13.78	13.79	13.77	13.31	16.08	16.64	16.79	16.82
	(b)	18.64	19.29	19.08	19.00	18.93	18.64	21.60	22.32	22.58	22.66
	(c)	18.64	19.26	18.99	18.87	18.78	18.64	21.57	22.22	22.44	22.50
	(d)	18.64	19.27	18.98	18.85	18.77	18.64	21.57	22.21	22.42	22.49



**Fig. 9.** Dryness rate of insulation assemblies with S/BP or HC under Nancy's and Marseille's climates.

kWh for HC and 2201 kWh and 1778 kWh for S/BP under Nancy's and Marseille's climates, respectively.

The additional insertion of the air layer in accordance with case (c), resulted in a further decrease in the total required annual energy consumption yielding 2260 kWh and 1807 kWh for HC and 2160 kWh and 1777 kWh for S/BP under Nancy's and Marseille's climates, respectively.

For case (d), a marginal decrease in energy consumption of 0.7 % for HC and 0.3 % for S/BP was observed Under Nancy's climate, in

comparison to case (c). Conversely, there was no observed improvement in energy consumption under Marseille's climate.

Furthermore, the S/BP bio-composite exhibited slightly better effectiveness compared to HC for thermal insulation use under the studied climatic conditions. This outcome was predicted, given that the thermal conductivity of HC is greater than that of S/BP.

**4.2.1.2. Dryness rate.** The initial RH was set at 80 % for all various components comprising the insulation assemblies.

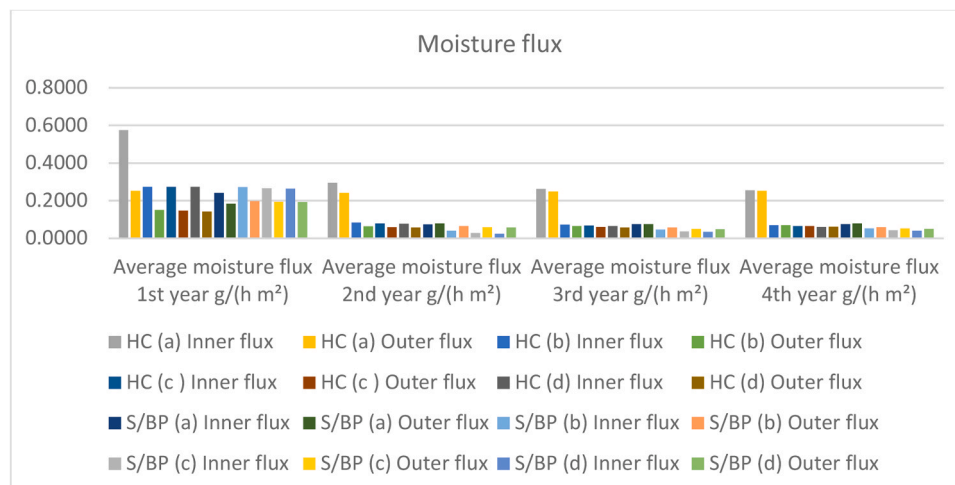


**Fig. 10.** Annual mean inner and outer moisture flux throughout both sides of insulation wall assemblies made of either S/BP or HC under Nancy's climate.

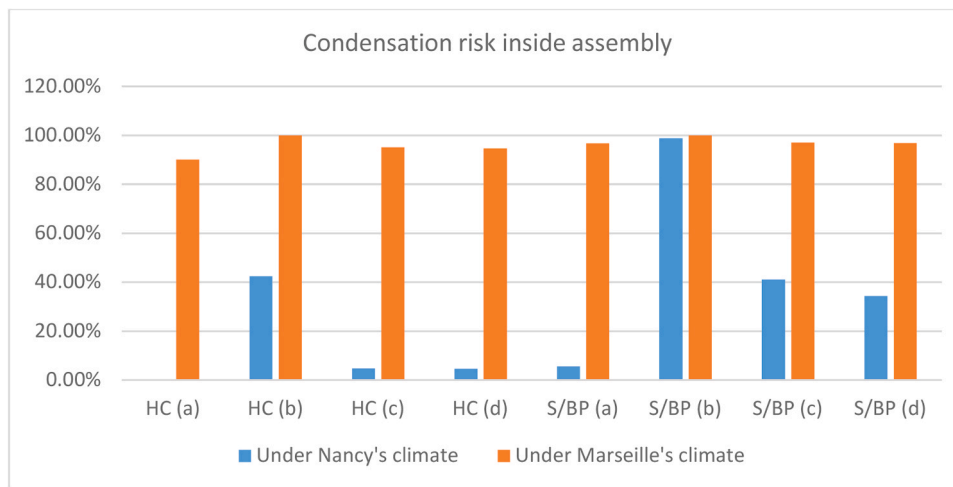


Fig. 11. Condensation risk inside insulation assemblies with S/BP or HC under Nancy's and Marseille's climates.

The total water content for each assembly was documented initially and subsequently after each year for a total duration of 4 years. The outcomes of these studies are outlined in Table 12. As a result, the dryness rate for each assembly was calculated and subsequently depicted graphically, as illustrated in Fig. 9.

Under Nancy's climate, the TWC of Insulation assemblies based on HC initially increased, eventually reaching a quasi-steady state after 4 years for the four cases. In contrast, TWC of insulation assemblies based on S/BP exhibited an initial increase, followed by the attainment of a quasi-steady-state after 4 years for only case (a). Whereas, the TWC for the remaining 3 cases began to gradually decrease progressively after the first year, reflecting the increased abilities of these assemblies to re-release accumulated moisture with their surroundings. These findings are consistent with the computed results regarding the annual mean inner and outer moisture flux entering and leaving the studied insulation assemblies, as shown in Fig. 10.

Conversely, the TWC is about 20 % higher for each case when considering Marseille's climate in comparison to that of Nancy. The TWC showed a continuous, gradual increase over the 4 years, reflecting the reduced abilities of these assemblies to dry out under Marseille's climate and resulting in the accumulation of moisture internally. This, in turn, heightens the risk of bio-deterioration mold, and decay damages within this structure.

For Nancy's conditions, insulation assemblies based on S/BP demonstrated less moisture absorption in comparison to Marseille's climate. For cases (a), (b), (c) and (d), the DR was equal to -3.4 %,

Table 13

Time lag and decrement factor of insulation assemblies with S/BP or HC under Nancy's and Marseille's climates based on inside and outside surface temperatures.

Conf.	Case	Under Nancy's climate		Under Marseille's climate	
		Time lag $\phi$ (h)	Decrement factor f (dimensionless)	Time lag $\phi$ (h)	Decrement factor f (dimensionless)
Primary	0	7	0.1273	10	0.0932
Insulation material based on Hemp concrete	(a)	6	0.0809	7	0.0432
	(b)	6	0.0831	7	0.0415
	(c)	6	0.0825	7	0.0411
	(d)	6	0.0825	7	0.0411
Insulation material based on Starch/Beet pulp	(a)	6	0.0825	6	0.0410
	(b)	6	0.0896	6	0.0470
	(c)	6	0.0894	6	0.0459
	(d)	6	0.0825	6	0.0458

-1.59 %, -0.79 %, and -0.72 %, respectively under Nancy's climate while they were notably lower at -26.37 %, -21.6 %, -20.74 %, -20.65 % under Marseille's climate. This can be attributed to the higher levels of absolute humidity in Marseille's climate compared to those in Nancy. Consequently, higher relative humidity levels will occur in indoors, resulting in an increase in the TWC within the assembly and a subsequent decrease in the DR.

Whereas, the Insulation assemblies based on HC exhibited DR values of -9.63 %, -11.01 %, -11.12 %, and -11.48 % for the same cases respectively under Nancy's climate, and substantially worse values of -34.15 %, -34.04 %, -33.90 %, -34.15 % under Marseille's climate.

It can be deduced that Insulation assemblies based on S/BP exhibited a lower moisture absorption rate compared to HC under both Nancy's and Marseille's climates. This can be attributed to the higher thermal insulation of S/BP, which helps raise the average temperature within the wall and therefore delays saturation and enhances dryness.

4.2.1.3. Condensation risk. All studied cases exhibited a complete absence of condensation risk on the internal surfaces of diverse assemblies. However, internal condensation risks manifested within the studied assemblies under both Nancy's and Marseille's climate. These risks were assessed by calculating the proportion of time during which criteria A, B, or C [38] were not satisfied. The results of these studies are illustrated in Fig. 11.

Increasing insulation thickness from 10 cm to 20 cm, resulted in a CR increase for HC from 0 % to 42.46 % under Nancy's climate and from 90.05 % to 100 % under Marseille's climate. Incorporating 2 cm and 4 cm air layers in the assembly led to a more effective decrease in CR, reducing it to 4.79 % and 4.63 % respectively under Nancy's climate. However, a minor decrease in CR to only 95.03 % and 94.66 % under Marseille's climate was observed after adding the 2 cm and 4 cm air layers, respectively.

As for S/BP, increasing insulation thickness from 10 cm to 20 cm increased CR from 5.61 % up to 98.78 % under Nancy's climate and from 96.67 % to 100 % under Marseille's climate. Incorporating 2 cm and 4 cm air layers in these assemblies led to a minor decrease in CR to 95.03 % and 94.66 % under Nancy's climate and 96.98 % and 96.79 % under Marseille's climate, respectively.

It can be deduced that Insulation assemblies based on S/BP exhibited higher CR within the wall compared to HC for the same assembly configuration under both analyzed climatic conditions. This can be attributed to the elevated water vapor permeability of HC in contrast to S/BP.

Furthermore, it was noted that a higher CR was consistently observed under Marseille's climate for the same studied configuration due to the

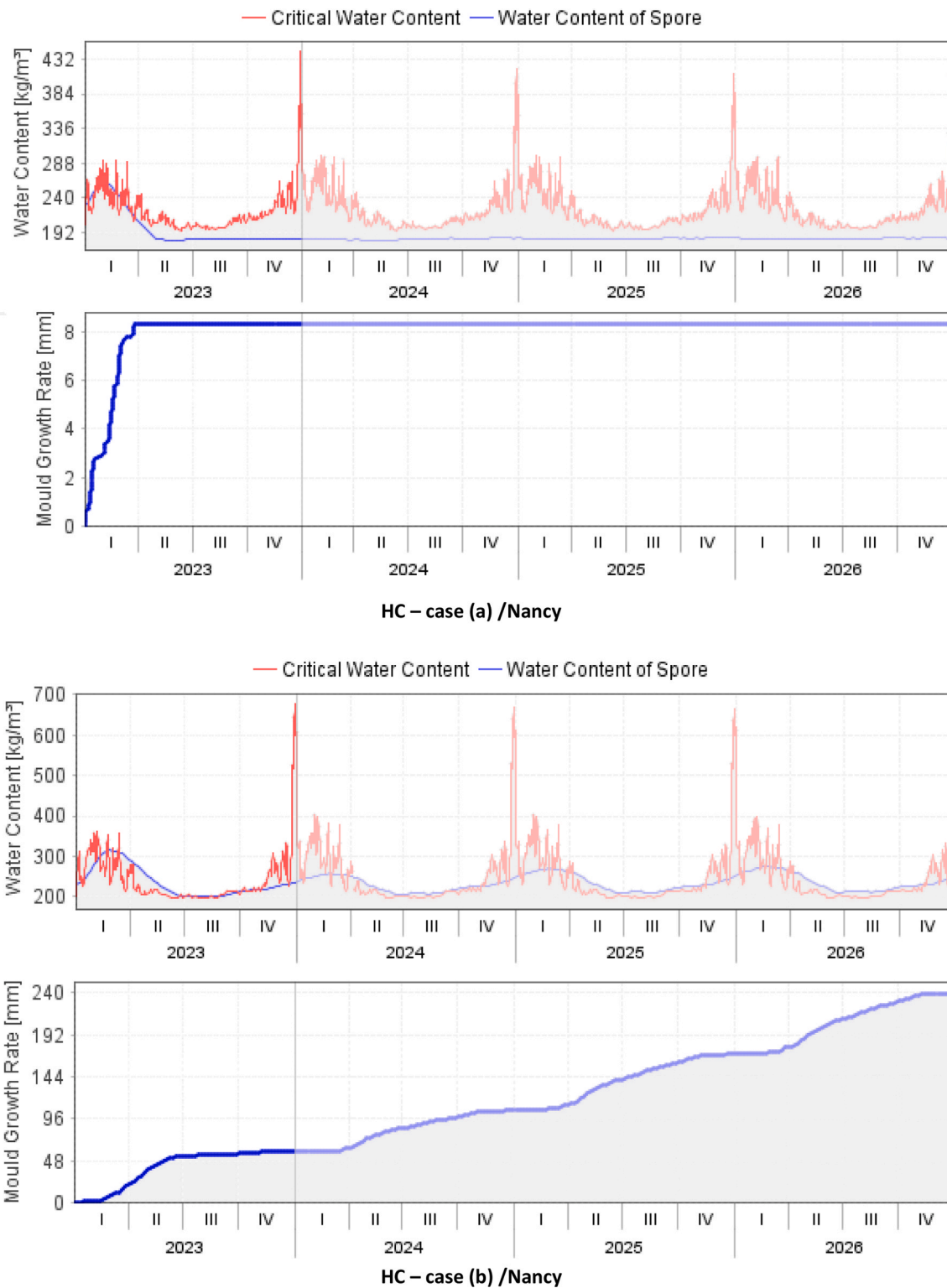


Fig. 12. Water content and mold growth rate for various insulation assemblies with HC under Nancy's climate. HC- case (a,b,c,d).

increased frequency in days with higher absolute humidities compared to Nancy's climate. Lastly, the less detrimental CR was observed for case (a) for both insulation assemblies based on S/BP and HC under Nancy's climate.

4.2.1.4. *Dynamic thermal behavior.* Optimizing the dynamic thermal behavior is essential to achieve a higher time lag and a lower decrement

factor. This can be realized through increasing wall thickness and reducing its overall thermal diffusivity, which involves minimizing the thermal diffusivities of the individual layers constituting the wall. For this purpose, the time lag and decrement factor for each assembly were documented. The outcomes of these studies are outlined in Table 13.

Insulation materials based on HC exhibited a time lag of around 6 hours under Nancy's climate and around 7 hours under Marseille's



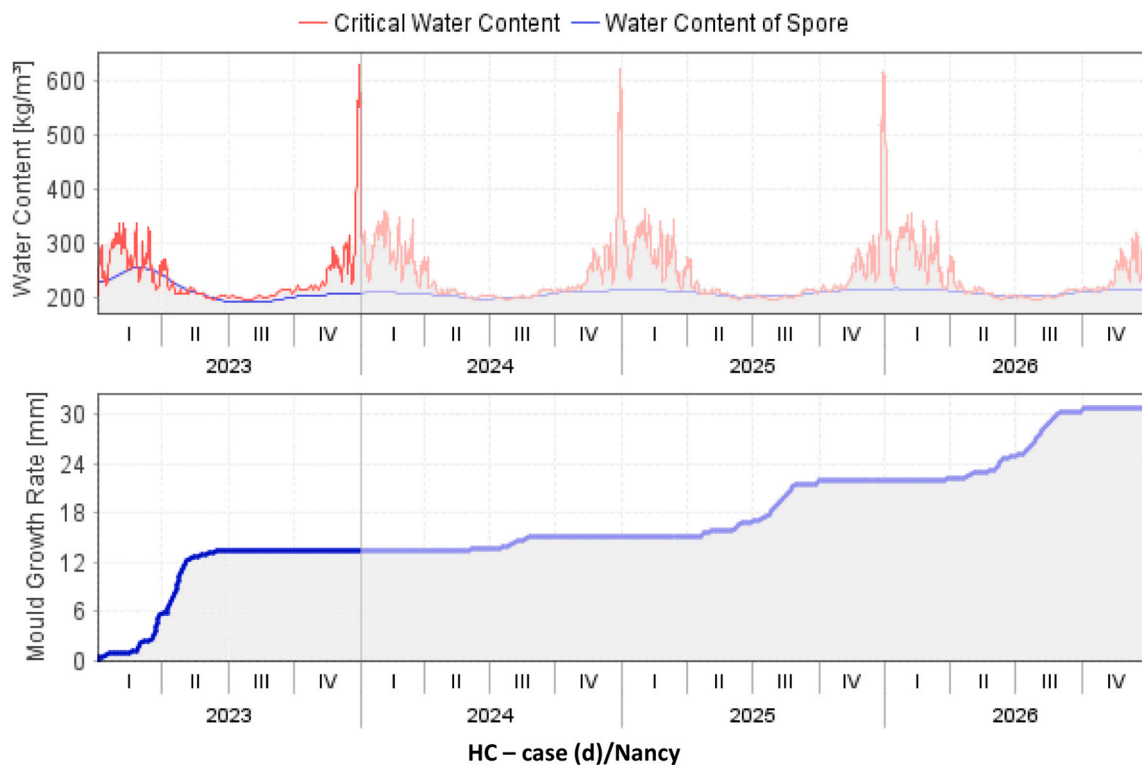
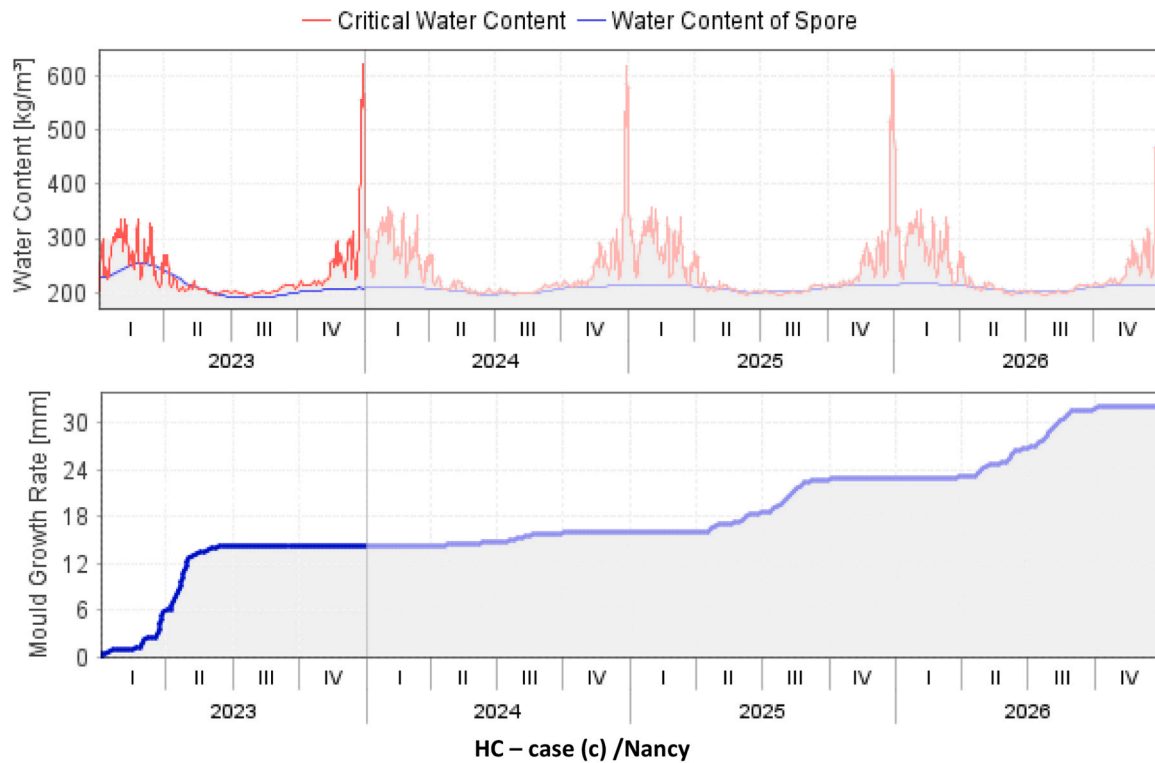


Fig. 12. (continued).

climate. However, Insulation materials based on S/BP exhibited a time lag of around 6 hours under both Nancy’s and Marseille’s climates.

As for the decrement factor, the increase of insulation thickness from 10 cm to 20 cm under Nancy’s climate resulted in its increase from 0.0809 to 0.0831 and from 0.0825 to 0.0896 for insulation assemblies based on HC and S/BP respectively. Conversely, a reduction in the decrement factor was observed after the incorporation of air layers as it

reached 0.0825 for Insulation materials based on HC and S/BP for an air layer of 4 cm. This is expected, as the incorporation of air layers induces an increase in the thermal resistance of the assembly.

However, within the climatic conditions of Marseille, a substantial reduction in decrement factor was noted when compared to Nancy’s climate. This reduction averaged 49.2 % and 47.8 % for insulation assemblies with HC and S/BP respectively. This is attributed to the

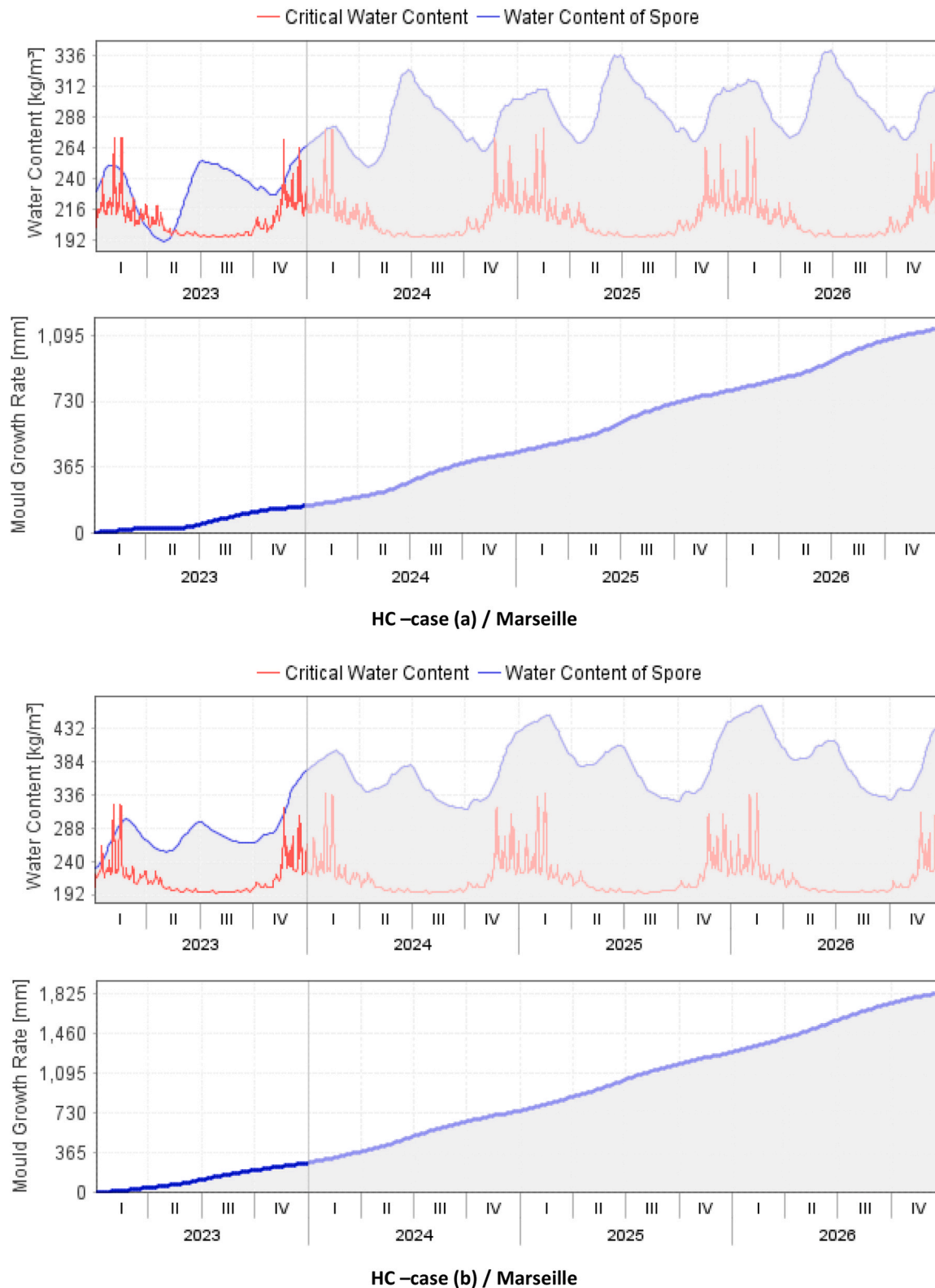


Fig. 13. Water content and mold growth rate for various insulation assemblies with HC under Marseille’s climate. HC– case (a,b,c,d).

elevated total water content within the assembly in Marseille’s climate compared to Nancy’s climate. This increase in TWC augments the thermal mass of the assembly, enabling the storage of a greater amount of thermal energy and exhibiting therefore a damping effect on the decrement factor.

Notably, the acquired values of time lag and decrement factor are significantly impacted by the control of indoor air temperature through the imposed air conditioning system.

Eventually, Insulation assemblies based on S/BP and HC showcased enhanced dynamic thermal behavior under Marseille’s climates.

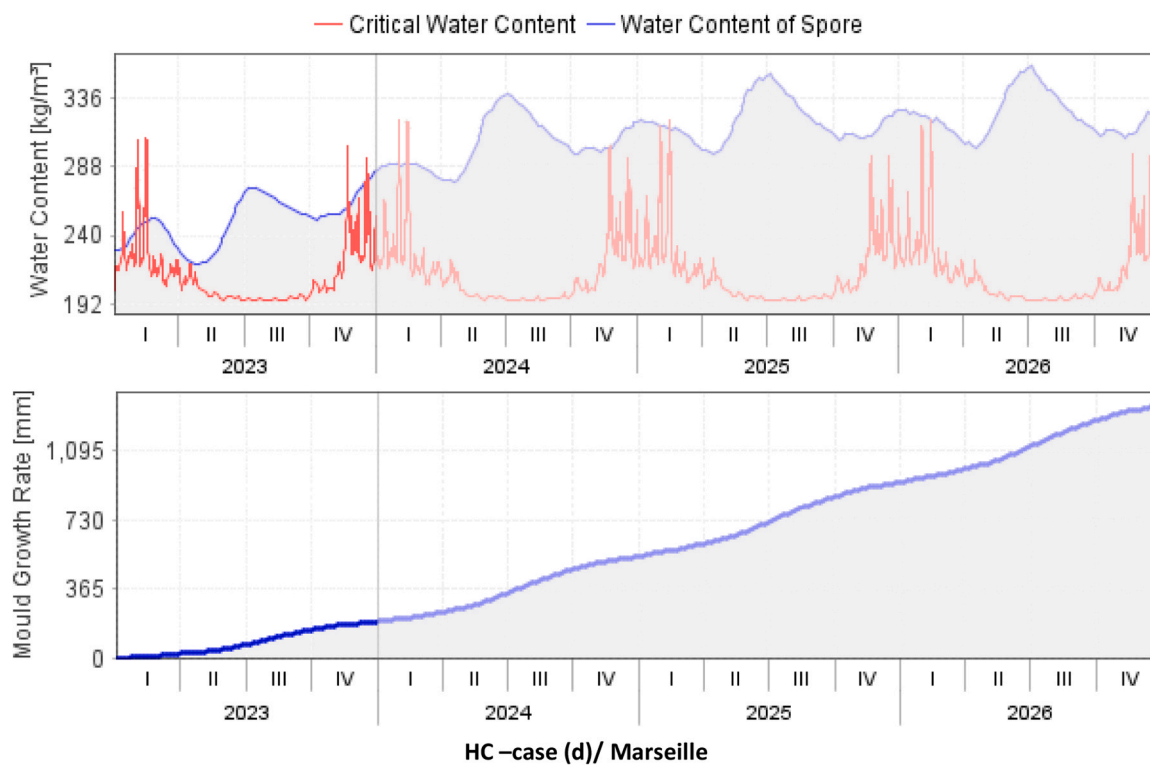
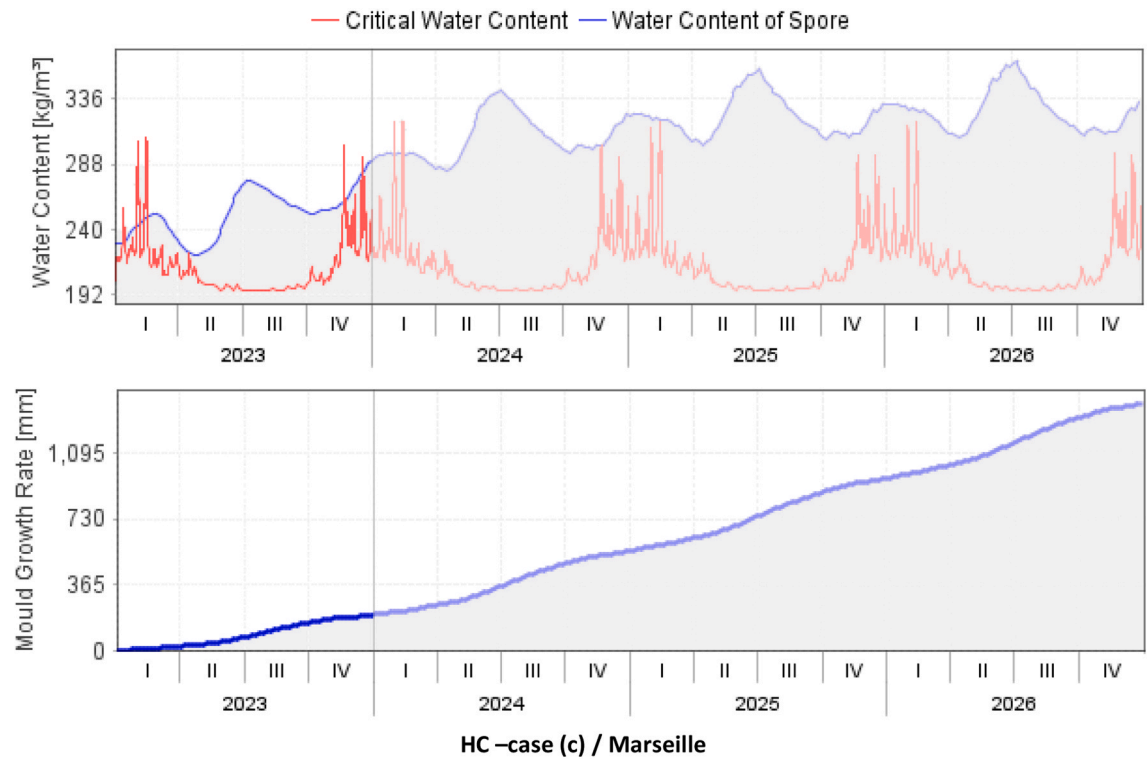


Fig. 13. (continued).

Notably, the best time lag and decrement factor were observed for case (d) for insulation assembly with HC and for case (a) for insulation assembly with S/BP.

4.2.2. WUFI-Bio mold growth risk assessment

The most essential factors affecting mold growth are the temperature, the relative humidity, and the substrate quality which is considered

class I in this study, denoting for bio-utilizable substrates. The WUFI®Bio software determines the hourly critical water content which depends on the imported hourly temperatures and the selected substrate class.

For this reason, this software looks up the relative humidity above which, according to the Lowest Isoleth for Mold growth (LIM) of the selected substrate class, germination or growth becomes possible at the

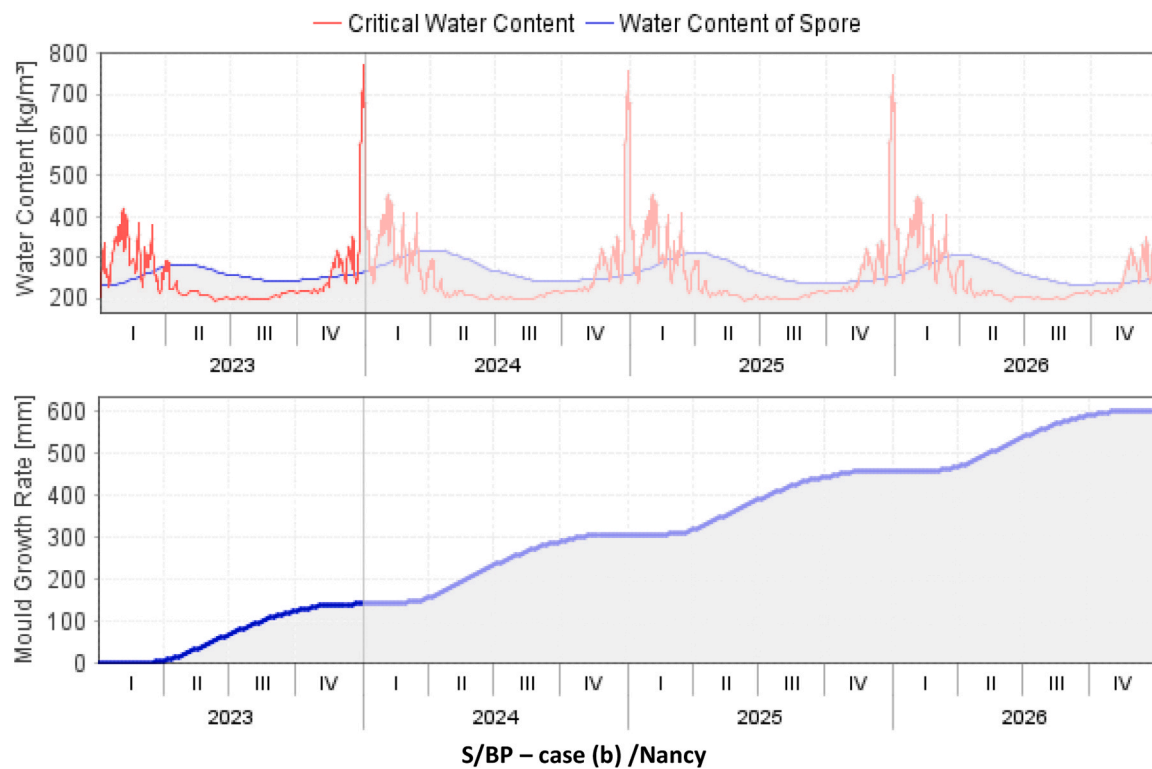
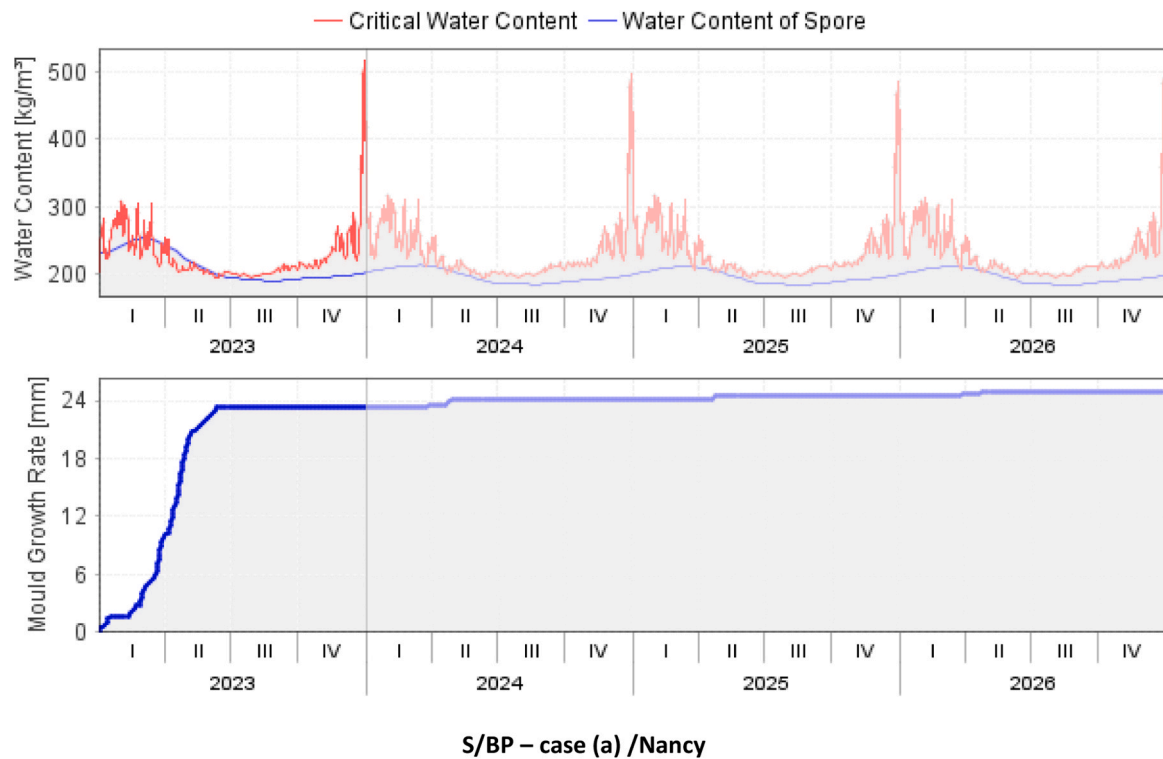


Fig. 14. Water content and mold growth rate for various insulation assemblies with S/BP under Nancy’s climate. S/BP– case (a,b,c,d).

current ambient temperature. This relative humidity is then converted to the critical water content, using the moisture storage function of the spore. As soon as the water content in the spore exceeds this critical water content, the relative humidity of its contents has exceeded the LIM, and it is assumed that either the spore germinates and mycelium

growth begins, or, if the spore has germinated previously, mycelium growth resumes.

Therefore, the difference in configurations among the four wall assemblies will induce variations in the hourly imported temperature and water content across the bio-composite material layer. Consequently,

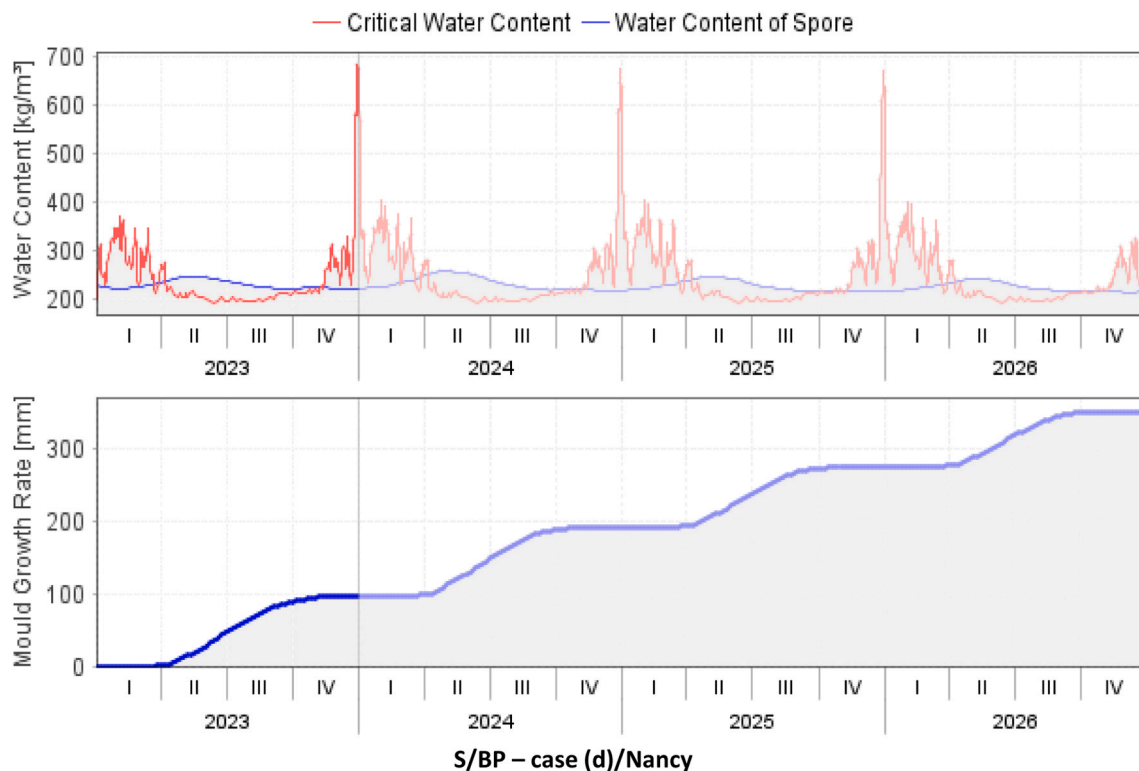
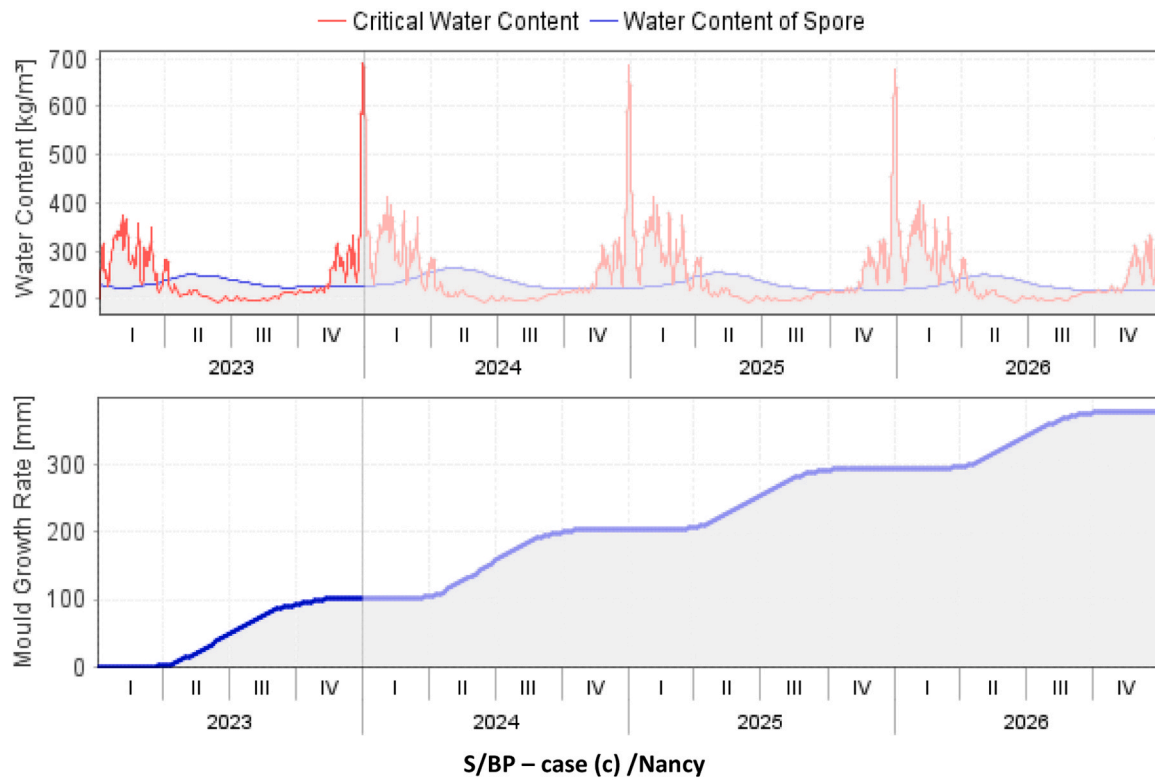


Fig. 14. (continued).

this will impact the water content in spores and modify the critical water content profiles, thereby directly influencing the risk of mold growth.

The fluctuations in water content within the spore with time, the critical water content for mycelium germination, and the mold growth rate for each insulation assembly based on HC over 4 years are illustrated in Figs. 12 and 13 under Nancy’s and Marseille’s climates,

respectively. Conversely, the aforementioned studies conducted on insulation assemblies based on S/BP are illustrated in Figs. 14 and 15 under the respective studied climates.

Furthermore, the signal light provides a comprehensive evaluation of the potential mold growth risk and the severity of the infestation if present. For an occupant exposition class, which in this study pertains to

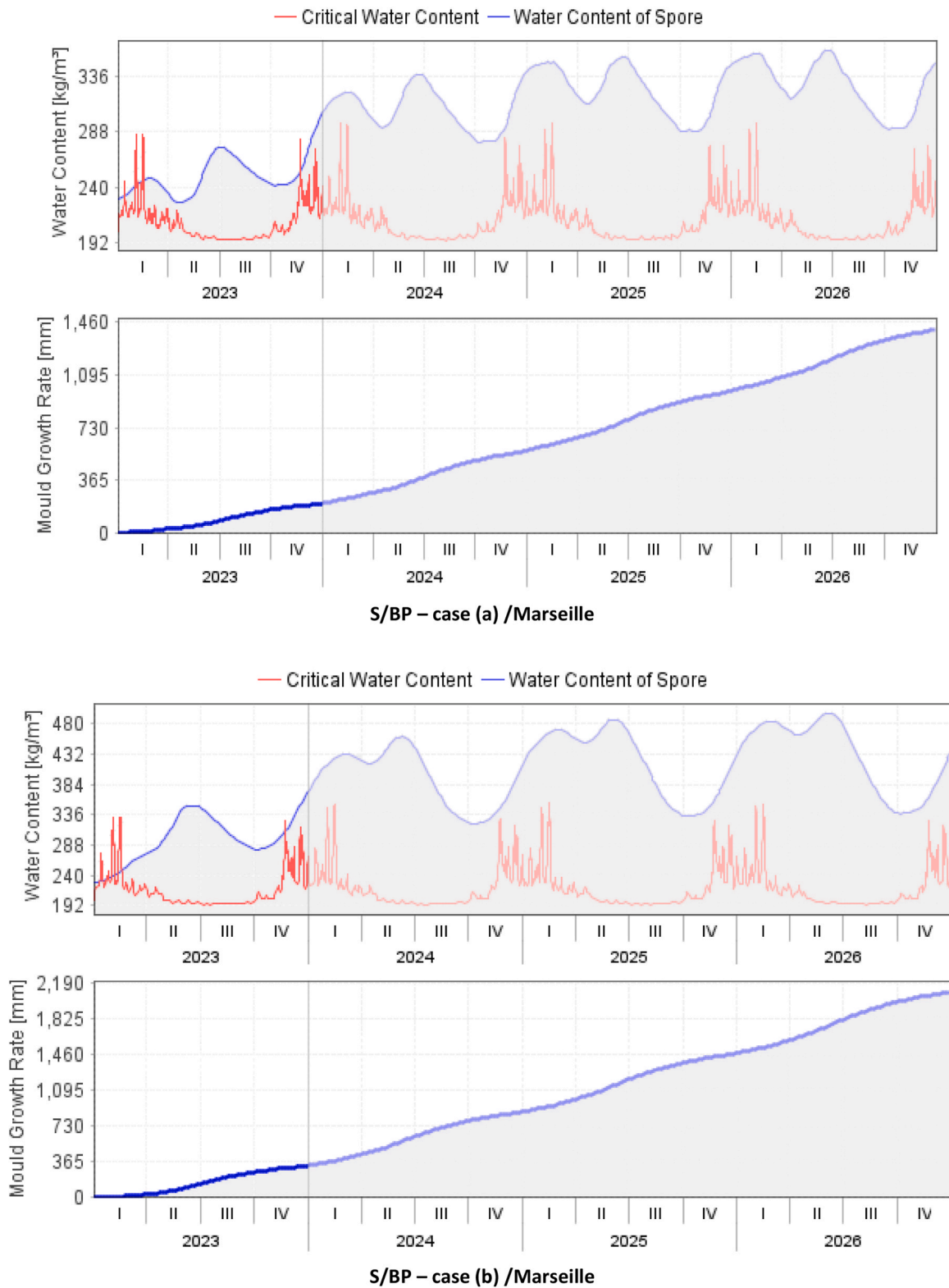


Fig. 15. Water content and mold growth rate for various insulation assemblies with S/BP under Marseille's climate. S/BP – case (a,b,c,d).

surfaces inside constructions without direct contact with indoor air, if the mold growth rate (MGR) falls within the range of 176–239 mm/year and the mold index (MI) is between 2 and 3, a yellow signal light is displayed. This signifies the need for further criteria of investigations to assess safety and acceptability. Conversely, when the values fall below

these thresholds, the signal light turns into green, denoting acceptability. However, exceeding these values causes the signal light to turn red, indicating that the structure is at a significantly elevated risk of mold growth, rendering it unacceptable.

In this context, the MGR, MI, and signal light of insulation assemblies

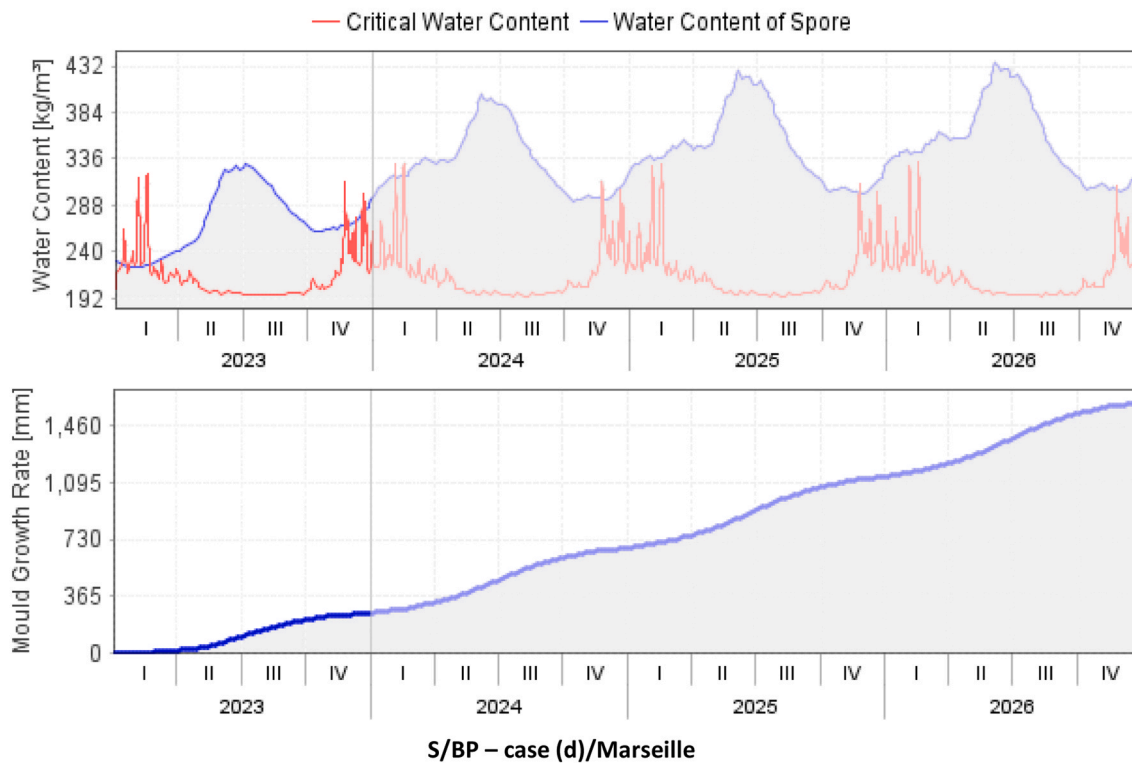
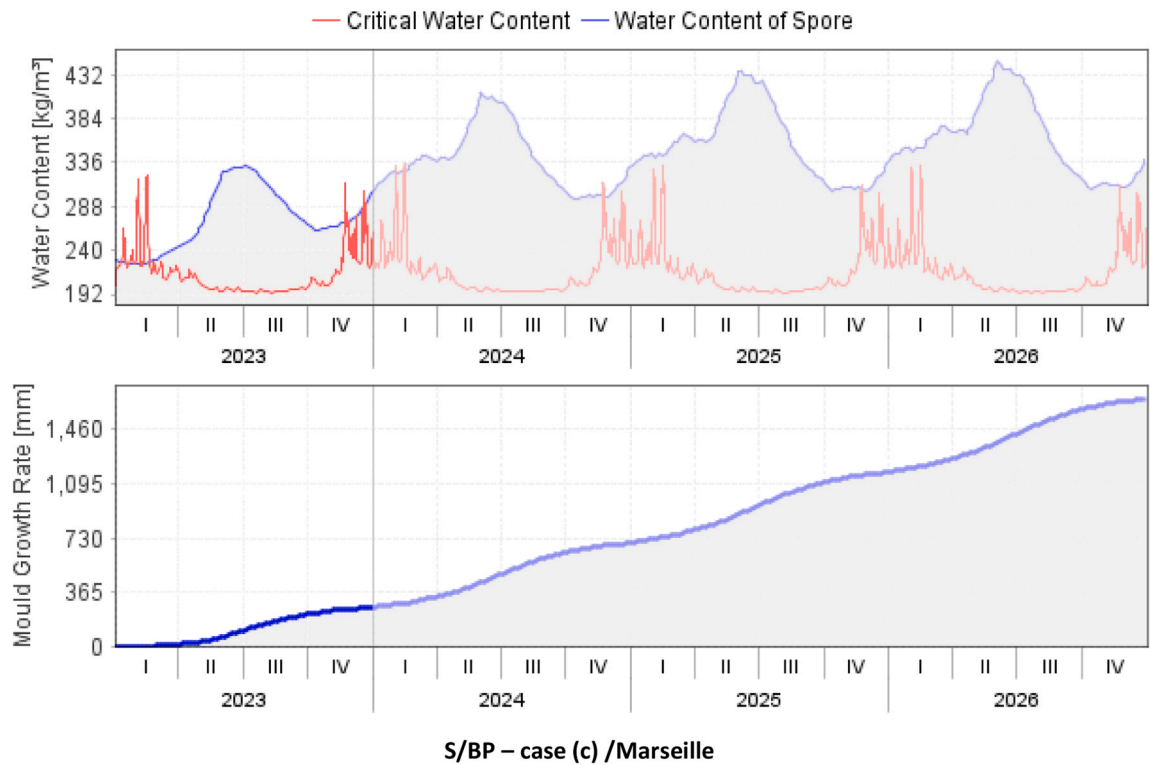


Fig. 15. (continued).

based on S/BP or HC under Nancy’s and Marseille’s climates are outlined in Table 14.

As stated before, it has been observed that mold growth increased when the water content within the spores exceeded the critical water content, and remained stable elsewhere, as reflected in Figs. 12–15.

Under Nancy’s climate, all insulation assemblies exhibited a green signal light, affirming their acceptability. The increase in insulation

thickness from 10 cm to 20 cm led to an increase in the MI from 0.01 to 0.16 for Insulation assemblies based on HC and from 0.05 to 1.25 for Insulation materials based on S/BP. This can be attributed to the increase in moisture absorption and to the prolonged periods of moisture retention due to the increase in bio-insulation material thickness.

The integration of the air layer proved effective in reducing MI to 0.02 and 0.45 for Insulation assembly based on HC and S/BP

**Table 14**

Mold growth rate, Mold index, and signal light of insulation assemblies with S/BP or HC under Nancy's and Marseille's climates.

Conf.	Case	Under Nancy's climate			Under Marseille's climate		
		MGR (mm/year)	MI (dimensionless)	Signal light	MGR (mm/year)	MI (dimensionless)	Signal light
Insulation material based on Hemp concrete	(a)	8.35	0.01	Green	149	1.45	Green
	(b)	57.8	0.16	Green	271	3.39	Red
	(c)	14.2	0.03	Green	198	2.4	Yellow
	(d)	13.4	0.02	Green	194	2.33	Yellow
Insulation material based on Starch/Beet pulp	(a)	23.3	0.05	Green	207	2.54	Yellow
	(b)	140	1.25	Green	323	3.92	Red
	(c)	100	0.51	Green	264	3.31	Red
	(d)	95.9	0.45	Green	256	3.22	Red

respectively and for an air layer thickness of 4 cm. This can be attributed to the role of the air layer as a barrier, effectively isolating the interior surfaces of the assembly from the exterior moisture sources which helps in reducing the available moisture and maintaining a more stable environment.

Under Marseille's climate, exclusively case (a) for insulation assemblies based on HC exhibited a green signal light with a MI value of 1.45. Whereas, case (b) displayed a red light with a maximum MI value of 3.39, while cases (c) and (d) displayed a yellow signal light. As for insulation assemblies based on S/BP, case (a) displayed a yellow signal light with a MI value of 2.54. Whereas the remaining cases signaled a red light with a maximum MI value of 3.92 for case (b).

Hence, Insulation assemblies based on HC showcased lower susceptibility to mold growth risk in comparison to insulation assemblies based on S/BP under both studied climatic conditions. This outcome was anticipated, given that HC has a higher water vapor permeability than S/BP which prevents moisture accumulation and enables even moisture distribution and redistribution within the assembly, resulting in a reduced risk of mold growth. Furthermore, the risk of mold growth was found to be less pronounced under Nancy's climate which can be attributed to the increased frequency in days with higher absolute humidities in Marseille compared to Nancy's climate.

## 5. Conclusion

Initially, this study assessed the hygrothermal characteristics of an economically viable, bio-derived material made of starch and beet pulp with a mass ratio equal to 40 % for building insulation use. For this purpose, experimental studies were elaborated to determine the water vapor resistance factor under elevated humidities, capillary absorption coefficient, moisture content at free saturation, and thermal conductivity dependent on humidity. The results indicated favorable hygrothermal performance, rendering this material suitable for employment in internal building insulation. However, it was found unsuitable for external insulation use.

Afterward, a comprehensive evaluation and comparison of the hygrothermal performances and mold growth risk assessment of different multilayer insulation assemblies made of either Starch/Beet pulp or Hemp concrete were undertaken. This analysis entailed numerical simulations utilizing the WUFI® Plus and WUFI®Bio softwares, conducted within the climatic conditions of two distinct cities in France-Nancy and Marseille. The primary goal was to investigate the influence of insulation materials types, thickness, covering materials, and the presence of an air layer on indoor hygrothermal comfort across varying outdoor weather conditions.

For each design, the overall energy performance, total water content, drying rate, condensation risk, and mold growth were evaluated. The objective was to associate with each specific climate the optimal assembly configuration from both hygric and thermal perspectives.

Results showed that insulation assemblies based on the:

- S/BP bio-composite exhibited better effectiveness compared to HC for potential energy savings in thermal insulation. This was

particularly notable under Nancy's climate, with case (d) proving to be the most advantageous configuration.

- S/BP bio-composite exhibited a better dryness rate compared to HC. This was particularly notable under Nancy's climate, with case (d) proving to be the most advantageous configuration.
- S/BP bio-composite exhibited higher CR within the wall compared to HC. The less severe CR for S/BP was observed for case (a) under Nancy's climate.
- HC composite showcased better dynamic thermal behavior compared to S/BP, particularly under Marseille's climate. Notably, among all cases associated with S/BP, case (a) under Marseille's climate, proved to be the better configuration when considering both the time lag and decrement factor perspectives.
- HC composite showcased lower susceptibility to mold growth risk compared to S/BP, particularly under Nancy's climate. Notably, among all cases associated with S/BP, case (a) under Nancy's climate, proved to be the most advantageous configuration when considering both MGR and MI perspectives.

In conclusion, insulation assemblies based on S/BP demonstrated more advantageous hygrothermal performance under Nancy's climate compared to that of Marseille. A more pronounced reduction in energy consumption, a decreased lower and more stable total water content variation, a reduced moisture absorption, a reduced condensation risk, and a lower susceptibility to mold growth were observed under Nancy's climate for insulation assemblies based on S/BP. Conversely, the only notable improvement observed for these assemblies was a more favorable decrement factor under Marseille's climate. These results can be mainly attributed to the heightened frequency in days characterized by higher absolute humidity levels in Marseille compared to Nancy's climate.

## CRedit authorship contribution statement

**Elias Harb:** Writing – review & editing, Writing – original draft, Visualization, Validation, Software, Methodology, Investigation, Formal analysis, Data curation, Conceptualization. **Christophe Bliard:** Writing – review & editing, Visualization, Validation, Supervision, Resources, Project administration, Methodology, Investigation, Funding acquisition, Formal analysis, Data curation, Conceptualization. **Chadi Maa-louf:** Writing – review & editing, Visualization, Validation, Supervision, Software, Resources, Project administration, Methodology, Investigation, Funding acquisition, Formal analysis, Data curation, Conceptualization. **Mohammed Lachi:** Resources, Methodology, Investigation, Data curation, Conceptualization. **Elias Kinab:** Project administration. **Guillaume Polidori:** Writing – review & editing, Visualization, Validation, Supervision, Software, Resources, Project administration, Methodology, Investigation, Funding acquisition, Formal analysis, Data curation, Conceptualization.

## Declaration of Competing Interest

The authors declare that they have no known competing financial



interests or personal relationships that could have appeared to influence the work reported in this paper.

## Data availability

No data was used for the research described in the article.

## Acknowledgment

The authors would like to thank Crystal Union Company for providing the beet pulp necessary for the specimen manufacturing.

## References

- [1] European Commission Energy efficiency in buildings. Retrieved May 24, 2023, 2020 from [https://commission.europa.eu/news/focus-energy-efficiency-buildings-2020-02-17\\_en..](https://commission.europa.eu/news/focus-energy-efficiency-buildings-2020-02-17_en..)
- [2] H. Omrany, A. GhaffarianHoseini, A. GhaffarianHoseini, K. Raahemifar, J. Tookey, Application of passive wall systems for improving the energy efficiency in buildings: A comprehensive review, *Renew. Sustain. Energy Rev.* 62 (2016) 1252–1269, <https://doi.org/10.1016/j.rser.2016.04.010>.
- [3] F. Ascione, N. Bianco, G. Maria Mauro, D.F. Napolitano, Building envelope design: Multi-objective optimization to minimize energy consumption, global cost, and thermal discomfort. Application to different Italian climatic zones, *Energy* 174 (2019) 359–374, <https://doi.org/10.1016/j.energy.2019.02.182>.
- [4] Electricité de France. (n.d.). Il était une fois les réglementations thermiques. Retrieved May 24, 2023, from <https://particulier.edf.fr/fr/accueil/economies-d-energie/construction-et-renovation/la-reglementation-thermique-2012/il-etait-une-fois-les-reglementations-thermiques>.
- [5] Ministère de la transition écologique. (2023, February 17.). Réglementation environnementale RE2020. Retrieved May 24 2023, from <https://www.ecologie.gouv.fr/reglementation-environnementale-re2020>.
- [6] Y. Xue, Y. Fan, Z. Wang, W. Gao, Z. Sun, J. Ge, Facilitator of moisture accumulation in building envelopes and its influences on condensation and mold growth, *Energy Build.* 277 (2022) 112528, <https://doi.org/10.1016/j.enbuild.2022.112528>.
- [7] S. Li, X. Zhang, Y. Li, W. Gao, F. Xiao, Y. Xu, A comprehensive review of impact assessment of indoor thermal environment on work and cognitive performance - Combined physiological measurements and machine learning, *J. Build. Eng.* 71 (March) (2023) 106417, <https://doi.org/10.1016/j.job.2023.106417>.
- [8] K.A. Angelon-Gaetz, D.B. Richardson, S.W. Marshall, M.L. Hernandez, Exploration of the effects of classroom humidity levels on teachers' respiratory symptoms, *Int. Arch. Occup. Environ. Health* 89 (2016) 729–737, <https://doi.org/10.1007/s00420-016-1111-0>.
- [9] T. Menneer, M. Mueller, R.A. Sharpe, S. Townley, Modeling mold growth in domestic environments using relative humidity and temperature, *Build. Environ.* 208 (November 2021) (2022) 108583, <https://doi.org/10.1016/j.buildenv.2021.108583>.
- [10] H.J. Moon, S.H. Ryu, J.T. Kim, The effect of moisture transportation on energy efficiency and IAQ in residential buildings, *Energy Build.* 75 (2014) 439–446, <https://doi.org/10.1016/j.enbuild.2014.02.039>.
- [11] D. Kumar, M. Alam, P.X.W. Zou, J.G. Sanjayan, R. Ahmed, Comparative analysis of building insulation material properties and performance, *Renew. Sustain. Energy Rev.* 131 (March) (2020) 110038, <https://doi.org/10.1016/j.rser.2020.110038>.
- [12] C. Rabbat, S. Awad, A. Villot, D. Rollet, Y. André, Sustainability of biomass-based insulation materials in buildings: current status in France, end-of-life projections and energy recovery potentials, *Renew. Sustain. Energy Rev.* (2022) 156, <https://doi.org/10.1016/j.rser.2021.111962>.
- [13] C. Badouard, F. Bogard, C. Bliard, M. Lachi, B. Abbes, G. Polidori, Development and characterization of viticulture by-products for building applications, *Constr. Build. Mater.* 302 (July) (2021), <https://doi.org/10.1016/j.conbuildmat.2021.124142>.
- [14] M. Jerman, I. Palomar, V. Kočí, R. Černý, Thermal and hygric properties of biomaterials suitable for interior thermal insulation systems in historical and traditional buildings, *Build. Environ.* 154 (March) (2019) 81–88, <https://doi.org/10.1016/j.buildenv.2019.03.020>.
- [15] Y. Zhou, A. Trabelsi, M. El, Hygrothermal properties of insulation materials from rice straw and natural binders for buildings, *Constr. Build. Mater.* 372 (February) (2023) 130770, <https://doi.org/10.1016/j.conbuildmat.2023.130770>.
- [16] H.M. Künzel, Simultaneous Heat and Moisture Transport in Building Components – One- and Two-dimensional Calculation Using Simple Parameters (Ph.D. Thesis), Fraunhofer Institute of Building Physics, Stuttgart, Germany, 1995.
- [17] Fraunhofer Institute for Building Physics IBP.WUFI Passes Benchmark Test of EN 15026: WUFI Complies with the General Requirements of Standard EN 15026 and Passes its Benchmark Test (2007).
- [18] DIN EN 15026, Hygrothermal performance of building components and building elements – Assessment of moisture transfer by numerical simulation CEN, Brussels, Belgium (2007).
- [19] J. Lee, S. Wi, S. Jin, J. Choi, S. Kim, Prediction evaluating of moisture problems in light-weight wood structure: perspectives on regional climates and building materials, *Build. Environ.* 168 (July 2019) (2020) 106521, <https://doi.org/10.1016/j.buildenv.2019.106521>.
- [20] G. Tlajji, F. Pennec, S. Ouldboukhite, M. Ibrahim, P. Biwole, Hygrothermal performance of multilayer straw walls in different climates, *Constr. Build. Mater.* 326 (February) (2022) 126873, <https://doi.org/10.1016/j.conbuildmat.2022.126873>.
- [21] C. Feng, Y. Lei, J. Fang, B. Lu, X. Li, X. Xue, Optimized radiative parameters of building roof surfaces for energy efficiency: Case studies in China, *J. Build. Eng.* 61 (September) (2022) 105289, <https://doi.org/10.1016/j.job.2022.105289>.
- [22] S. Luzzi, C. Rubino, P. Stefanizzi, ScienceDirect. Use of clay and olive pruning waste for building materials with high hygrothermal performances Use of clay and pruning waste for building materials with high hygrothermal performances Assessing the feasibility of using the heat temperature function for district heat demand forecast, *Energy Procedia* 126 (2017) 234–241, <https://doi.org/10.1016/j.egypro.2017.08.145>.
- [23] S. Simon, S. Jiang, J.L. Hao, J.N. De Carli, Hygrothermal and mechanical performance of sustainable concrete: a simulated comparison of mix designs, *J. Build. Eng.* 34 (November 2019) (2021) 101859, <https://doi.org/10.1016/j.job.2020.101859>.
- [24] G.B.A. Coelho, H.E. Silva, F.M.A. Henriques, Calibrated hygrothermal simulation models for historical buildings, *Build. Environ.* 142 (May) (2018) 439–450, <https://doi.org/10.1016/j.buildenv.2018.06.034>.
- [25] S. Ho Ryu, H. Jun, J. Tai, Evaluation of the influence of hygric properties of wallpapers on mold growth rates using hygrothermal simulation, *Energy Build.* 98 (2015) 113–118, <https://doi.org/10.1016/j.enbuild.2014.09.058>.
- [26] A. Brambilla, E. Gasparri, Hygrothermal behavior of emerging timber-based envelope technologies in Australia: a preliminary investigation on condensation and mold growth risk, *J. Clean. Prod.* 276 (2020) 124129, <https://doi.org/10.1016/j.jclepro.2020.124129>.
- [27] Karaky, Hamzé. (2018). "Élaboration et Caractérisation Physique et Hygrothermique d'un Agro-Matériau à Base de Pulpe de Betterave et d'amidon." Thèse de l'Université de Reims-Champagne-Ardenne.
- [28] G. Costantine, E. Harb, C. Bliard, C. Maalouf, E. Kinab, B. Abbès, G. Polidori, Experimental characterization of starch/beet pulp bricks for building applications: Drying kinetics and mechanical behavior, *Constr. Build. Mater.* 264 (2020) 120270, <https://doi.org/10.1016/j.conbuildmat.2020.120270>.
- [29] E. Harb, C. Maalouf, C. Bliard, M. Tenpierik, M. Lachi, F. Bogard, G. Polidori, Thermal performance of starch/beet pulp composite bricks for building insulation at a wall scale, *Case Stud. Constr. Mater.* 18 (October 2022) (2023) e01851, <https://doi.org/10.1016/j.cscm.2023.e01851>.
- [30] M.J. Tenpierik, M. Lachi, C. Bliard, G. Polidori, Experimental and numerical investigation of the thermal inertia of sugar-beet pulp / starch based bricks enhanced with phase change materials, *Constr. Build. Mater.* 383 (March) (2023) 131367, <https://doi.org/10.1016/j.conbuildmat.2023.131367>.
- [31] H. Karaky, C.M. Id, C. Bliard, T. Moussa, N. Wakil, El, M. Lachi, G. Polidori, Hygrothermal and acoustical performance of starch-beet pulp composites for building thermal insulation, *Materials* 2018 (11) (2018) 1622, <https://doi.org/10.3390/ma11091622>.
- [32] H. Karaky, C. Maalouf, C. Bliard, A. Gacoin, M. Lachi, N. El, G. Polidori, Characterization of beet pulp fiber reinforced potato starch biopolymer composites for building applications, *Constr. Build. Mater.* 203 (2019) 711–721, <https://doi.org/10.1016/j.conbuildmat.2019.01.127>.
- [33] NF EN ISO 12572. (2016). Hygrothermal performance of building materials and products – Determination of water vapour transmission properties – Cup method. AFNOR 2016.
- [34] NF EN ISO 16535, Thermal insulation products for building applications – Determination of long term water absorption by immersion, AFNOR (2019) 2019.
- [35] WUFI®. (2019, April 16). WUFI® Plus software. Retrieved May 25, 2023, from <https://wufi.de/en/software/wufi-plus/>.
- [36] B. Seng, C. Magniont, S. Lorente, Characterization of a precast hemp concrete block. Part II: Hygric properties, *J. Build. Eng.* 24 (2018) (2019) 100579, <https://doi.org/10.1016/j.job.2018.09.007>.
- [37] B. Seng, C. Magniont, S. Lorente, Characterization of a precast hemp concrete. Part I: Physical and thermal properties, *J. Build. Eng.* 24 (2018) (2019) 100540, <https://doi.org/10.1016/j.job.2018.07.016>.
- [38] ASHRAE, 2008. Standard 160-2008. Criteria for Moisture-Control Design Analysis in Buildings. ASHRAE Transactions, 114 PART 1, 167–171, Atlanta, GA.
- [39] M. Ibrahim, P.H. Biwole, E. Wurtz, P. Achard, A study on the thermal performance of exterior walls covered with a recently patented silica-aerogel-based insulating coating, *Build. Environ.* 81 (2014) 112–122, <https://doi.org/10.1016/j.buildenv.2014.06.017>.
- [40] C.H. Koh, F. Gauvin, K. Schollbach, H.J.H. Brouwers, Investigation of material characteristics and hygrothermal performances of different bio-based insulation composites, *Constr. Build. Mater.* 346 (May) (2022) 128440, <https://doi.org/10.1016/j.conbuildmat.2022.128440>.
- [41] E. Latif, S. Tucker, M. Anca, D. Chitral, D. Newport, Hygric properties of hemp bio-insulations with differing compositions, *Constr. Build. Mater.* 66 (2014) 702–711, <https://doi.org/10.1016/j.conbuildmat.2014.06.021>.
- [42] NF EN ISO 15148. (2003). Hygrothermal performance of building materials and products – Determination of water absorption coefficient by partial immersion AFNOR 2003.
- [43] P. Monreal, L.B. Mboumba-Mamboundou, R.M. Dheilly, M. Quéneudec, Effects of aggregate coating on the hygral properties of lignocellulosic composites, *Cem. Concr. Compos.* 33 (2) (2011) 301–308, <https://doi.org/10.1016/j.cemconcomp.2010.10.017>.